THE PENNSYLVANIA STATE UNIVERSITY
SCHREYER HONORS COLLEGE

DEPARTMENT OF MECHANICAL ENGINEERING

BURNING RATES OF HAN AND HAN-METHANOL AT HIGH PRESSURES

EZEKIEL M. BUGAY
SPRING 2021

A thesis
submitted in partial fulfillment
of the requirements
for a baccalaureate degree
in Mechanical Engineering
with honors in Mechanical Engineering

Reviewed and approved* by the following:

Richard Yetter
Professor of Mechanical Engineering
Thesis Supervisor

Jean-Michel Mongeau
Assistant Professor of Mechanical Engineering
Honors Adviser

* Signatures are on file in the Schreyer Honors College.

ABSTRACT

A unique optical strand burner with very high-pressure capabilities was utilized to observe combustion behavior of 13M HAN and HAN-methanol solutions at constant pressures up to 70 MPa. These solutions were placed in respective 10.6 mm ID tubes and then ignited in the pressurized strand burner. High-speed videos of the sample were analyzed to derive a burning rate, which was plotted and then a predicting equation developed. After pressures of 30 MPa and until 70 MPa, it was found that both HAN-water and HAN-methanol propellants decreased in burn rate. Further, it was also determined that given the similarities in the results between the two propellants, HAN is likely the dominant component that governs the burn rate in this pressure regime. Unlike HAN-water, HAN-methanol exhibited a wide variety of flame behaviors across the tested pressures. The mechanisms of these behaviors are not yet known. It should be noted that the scope of this research was limited by the COVID-19 pandemic, and as such the data is not as great in quantity as it could have been otherwise.

TABLE OF CONTENTS

LIST OF FIGURES

LIST OF TABLES

ACKNOWLEDGEMENTS

I would like to thank Dr. Richard Yetter for accepting me into his lab as an undergraduate assistant and giving me help and guidance with this project, as well as teaching me a great deal about combustion and rocket propulsion. Further, I would like to thank Dr. Eric Boyer for significantly assisting me with technical issues and providing important context and insight. Finally, I would like to thank my peers Ryan Fritz and Eric Crisp for training me on the equipment, working with me to fix and modify things, and general help.

Chapter 1

Introduction

1.1 Research Motivations

Rocket propellants are exceptionally important to scientists and engineers—the characteristics of which directly affect performance, reliability, and safety of any given propulsion system. One of these propellant characteristics that is routinely scrutinized is the burning rate of the propellant. The burning rate, simply put, is the speed at which the combustion reaction occurs, visible and measurable by a moving flame surface. The burning rate of a propellant can dictate the flow rate through a nozzle, and by extension the thrust of a rocket motor [15].

The burning rate varies with changing pressure, as is evident from St. Robert's Law: $r_b = aP^n$, where P is pressure, a is a temperature-dependent constant, and n is a pressure-dependent exponent. However, it is becoming increasingly evident that St. Robert's Law cannot immediately be used to predict burning rates in extreme pressures or complex chemistry. Indeed, many studies on certain propellants show multiple burning regimes that could only have been obtained by empirical means [1, 3-5 ,16]. Consequently, a wealth of data is required so that correlations can be developed to assist scientists and engineers in predicting the behavior of these more complex scenarios.

One such family of propellants that is becoming increasingly explored is that of ionic monopropellants. Ionic monopropellants have a host of unique characteristics that are discussed in detail in Chapter 2, but in many cases lack sufficient burn rate data at extremes of pressure. Further, there is a shortage of equipment that is capable of both testing and observing combustion of these propellants at extremes of pressure [3, 4, 16]. Therefore, not only is exhaustive burn rate data necessary for these emerging propellants, but also visual data, so that engineers and scientists might better understand the underlying mechanisms of the combustion. Hydroxylammonium nitrate (HAN)-based monopropellants are one such family of ionic propellants that are under great interest, and the primary subject of this research.

1.2 Research Objectives

The primary goals of this research were to utilize the specialized Ultra-High-Pressure Optical Chamber (UHPOC) at Penn State's High-Pressure Combustion Lab (HPCL) to observe combustion phenomenon of HAN-based monopropellants at very high pressures, and then provide analysis and data using methods previously defined by Derk [16]. The objectives for this research are as follows:

- Modify the UHPOC and/or the operating procedure to accept HAN samples
- Perform combustion tests on and record video footage of HAN samples at increasing pressure starting at 30 MPa
- Analyze the data to determine burning rate trends and characteristics of HAN samples in the pressure range

1.3 Method of Approach

The UHPOC is a unique piece of machinery commissioned by the project's investigators, Dr. Richard Yetter and Dr. Eric Boyer. This equipment was designed and built, with the help of external vendors, to be an ultra-high-pressure optical strand burner—capable in theory of 300 MPa or more. The high-pressure and optical capabilities of this system make it especially suited for use in this research, where never-before-seen visual data of HAN combustion at extreme pressures is the focus.

Previous literature, discussed in Chapter 2, details the origins, characteristics, and benefits of ionic monopropellants. Among the literature, burning rates of HAN monopropellants at varying pressures is also addressed. Further, the UHPOC is explained and previous experiments on the equipment are discussed.

Chapter 3 focuses on the UHPOC machinery, function, and supporting equipment. In addition, this chapter describes the HAN formulations used in the experiment, as well as the sample preparation.

The procedure for operating the UHPOC test rig is explained in Chapter 4. Sample loading, machine preparation, pressurizing procedure, and unloading procedure are discussed.

Presenting the findings and analyzing the data is the subject of Chapter 5. In this chapter, a discussion takes place about the unusual burning rates of the tested HAN propellants, as well as the unusual flame behaviors of one of the propellants. Further, a CEA computer analysis is presented to calculate the flame temperatures present in the HAN reactions.

Finally, the conclusions and recommendations for future work are listed in Chapter 6. Discussions summarizing the findings and potential reasonings are also mentioned.

Chapter 2

Background and Review

2.1 Ionic Liquids and Propellants

Ionic liquids present unique opportunities for chemical propulsion. Defined as salts with melting points below 100°C that are used in the liquid state, ionic liquids can maintain their properties under extreme environmental conditions [9]. Within the last 30 years, ionic liquids have come under intense examination for use in monopropellants [1-14]. Hydrazine, a commonly used monopropellant, has come under scrutiny for its high volatility, sensitivity, and toxic and carcinogenic properties [2,8]. Several unique properties of ionic liquids address the issues currently experienced with hydrazine. The negligible vapor pressure of ionic liquids results in better handling characteristics—allowing for the liquid to be easily pumped, transported, and stored without special equipment. In other words, ionic liquids tend to have very low volatility [8,9]. In addition to low volatility, these ionic-liquid-based monopropellants tend be less environmentally harmful than hydrazine or its derivatives [2,8-10]. Many ionic propellants also maintain the same or exceed the combustion performance as hydrazine [10]. As such, monopropellants based on ionic liquids are among the best candidates for a hydrazine replacement.

Some of the most studied ionic liquids for use in monopropellants are Hydroxylammonium nitrate (HAN) and Ammonium dinitramide (ADN) [1,2,11-14]. HAN is a

salt which has a melting temperature of approximately 48°C, thus it can be easily made into an ionic liquid. Because of its high solubility of 95% [2], HAN is often mixed in an aqueous solution with a fuel to form a monopropellant, where it functions as the oxidizer [8,9]. HAN-based monopropellants were tested extensively by the United States Army Research Lab (ARL) in their liquid gun program [1,5]. The liquid gun program explored the application of high-energy monopropellants in firearms as a replacement for then-used (and still-used) solid propellants. Originating in the 1950s, the program was initially abandoned due to safety and handling concerns [5]. However, the liquid gun program was restarted in the 1980s and focused heavily on less-toxic, green fuels, such as HAN-based monopropellants [1].

ADN is also a salt with a relatively low melting point (93°C) and high solubility (70%). Like HAN, it is used as an oxidizer in aqueous form, in conjunction with a fuel, to form a monopropellant. ADN is especially notable for its low toxicity: this salt can come in contact with the eyes or skin without causing irritation [2]. ADN was of interest to various governments in the late 1980s and early 1990s as a replacement for highly-toxic ammonium perchlorate (AP) oxidizers in missile systems [6].

In the late 1990s and early 2000s attention had moved toward usage of HAN-based and ADN-based monopropellants in spacecraft [2, 7, 10-13]. HAN-based and ADN-based monopropellants are particularly of interest for spacecraft because of their high impulse density, which is sometimes in excess of 30% higher than hydrazine [2, 11]. This allows a spacecraft to have up to 40% less mass for the same performance as a hydrazine-powered craft [12].

2.2 Combustion Behavior of Ionic Monopropellants as Functions of Pressure

In addition to higher temperatures, future rocket engines may also need to perform at higher pressures in order to increase efficiency [13]. Therefore, many studies have emerged to research the behavior of ADN-based and HAN-based monopropellants at elevated pressures. Being ionic liquids, these monopropellants do not easily vaporize and combust in the gaseous phase. Rather, some studies suggest a liquid phase decomposition by the ionic oxidizer, and then a secondary decomposition by the fuel [1,7,14]. As one might expect, the nature of these decompositions varies tremendously between different formulations, temperatures, and pressures. In accordance with this variance, the behavior ionic propellants have proven difficult to predict [1,5,7,14,]. Over the last 20 years, many resources have been dedicated to gathering empirical data on ADN-based and HAN-based monopropellants so that they might be better understood.

A study by McBratney and Vanderhoff [1] examined the high-pressure combustion behavior of many gelled and un-gelled HAN-based monopropellants between 10 – 300 MPa. For XM46 propellant (a historically-studied formulation), temperature was also varied from -50 to 50°C. Table 1 lists all monopropellants tested with their respective percent compositions. Using an optical strand burner, McBratney and Vanderhoff recorded visual burn-rate data and regression. With the un-gelled propellants, it was noted that measured burn-rates were erratic at all pressures tested.

Table 1: Tested monopropellants and their percent compositions by McBratney & Vanderhoff [1].

Liquid Propellant	HAN	DEHAN	TEAN	Water
LP1845	63.2	0	20.0	16.8
XM46	60.8	0	19.2	20.0
LP4620	60.8	3.84	15.36	20.0
LP4640	60.8	7.68	11.52	20.0
LP1898	60.8	19.2	0	20.0
9.1 M HAN	60.8	0	0	39.2

The gelling of the propellants using 2% Kelzan or 1% Rhamsam (both fermentation polysaccharides) greatly increased the burning stability of the specimens and resulted in a planar burn surface between 80 – 300 MPa.

Special attention is given to the burn-rate vs. pressure data from this experiment. There are two distinct regions of burn-rate: the first region illustrates a general lack of pressure-dependence, while the second region shows a linear dependence on pressure. These results are stated to be in direct conflict with previous closed-bomb measurements with the same propellants. McBratney and Vanderhoff [1] refute any claims that the gelling of the propellants changed the burning characteristics of the tested propellants, saying that the XM46, when tested un-gelled at low temperatures, exhibited similar burn-rate characteristics. They continue to justify this by explaining that the burn-rates of the propellants had negligible temperature dependence at low pressures, since it was observed that the combustion behavior of XM46 was the same at low or ambient temperatures. The aforementioned burn-rate regions (as shown in Figure 1) were defined by a pressure break at approximately 70 MPa.

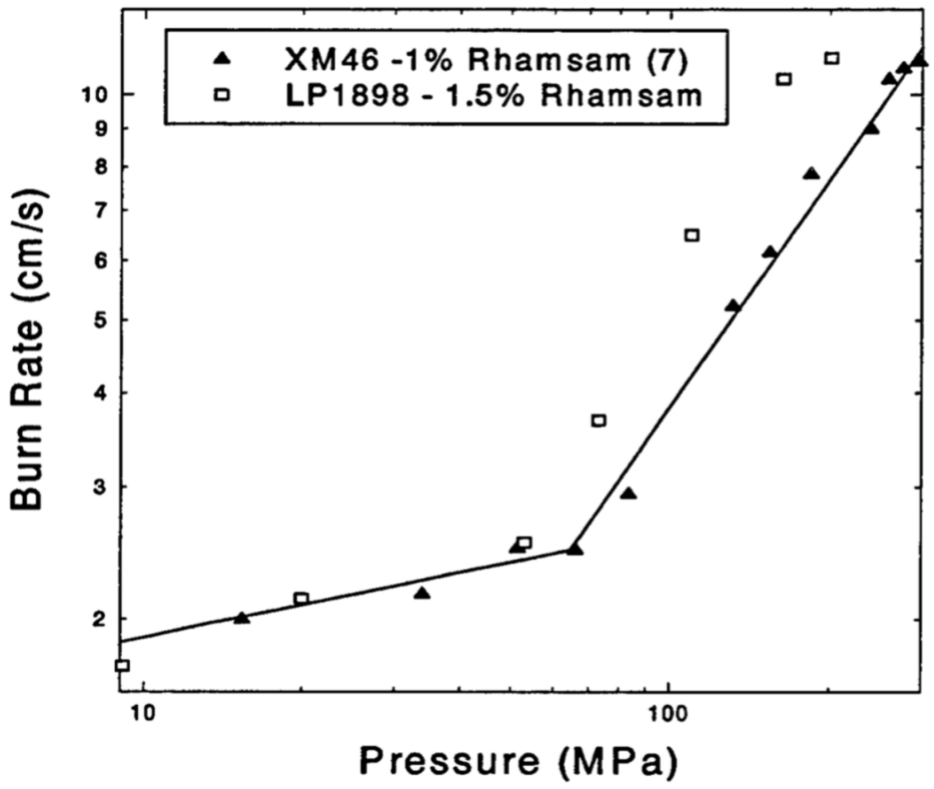

Fig. 1: Two distinct burn-rate regions for XM46 monopropellant [1].

Chang and Kuo [7] performed burn-rate experiments and chemical analysis on HANGLEY26, a more modern HAN-based monopropellant. Using a Liquid Propellant Strand Burner (LSPB), Chang and Kuo recorded visual combustion data on HANGLEY26 from 1.5 and 18.2 MPa. Like McBratney and Vanderhoff, Chang and Kuo noted two distinct pressure regions: the first between 1.5 – 8.8 MPa, and the second between 8.8 – 18.2 MPa. However, unlike the experiment by McBratney and Vanderhoff, Chang and Kuo found a much more erratic burn-rate function in the regions, leading them to define four distinct burning rate regimes. Figure 2 shows the four distinct burning rate regions of HANGLEY26 as a function of pressure.

To better interpret this burn-rate data, Chang and Kuo [7] evaluated the combustion byproducts of HANGLEY26. Chang and Kuo took samples of biproducts at each pressure tested, then plotted the molarity vs. pressure for each. The concentration of each major subspecies was statistically determined to be directly corelated with pressure. Chang and Kuo also found four distinct regimes for the subspecies concentration. Surprisingly, the concentration regimes closely corelated with the distinct burning regimes shown in Figure 2.

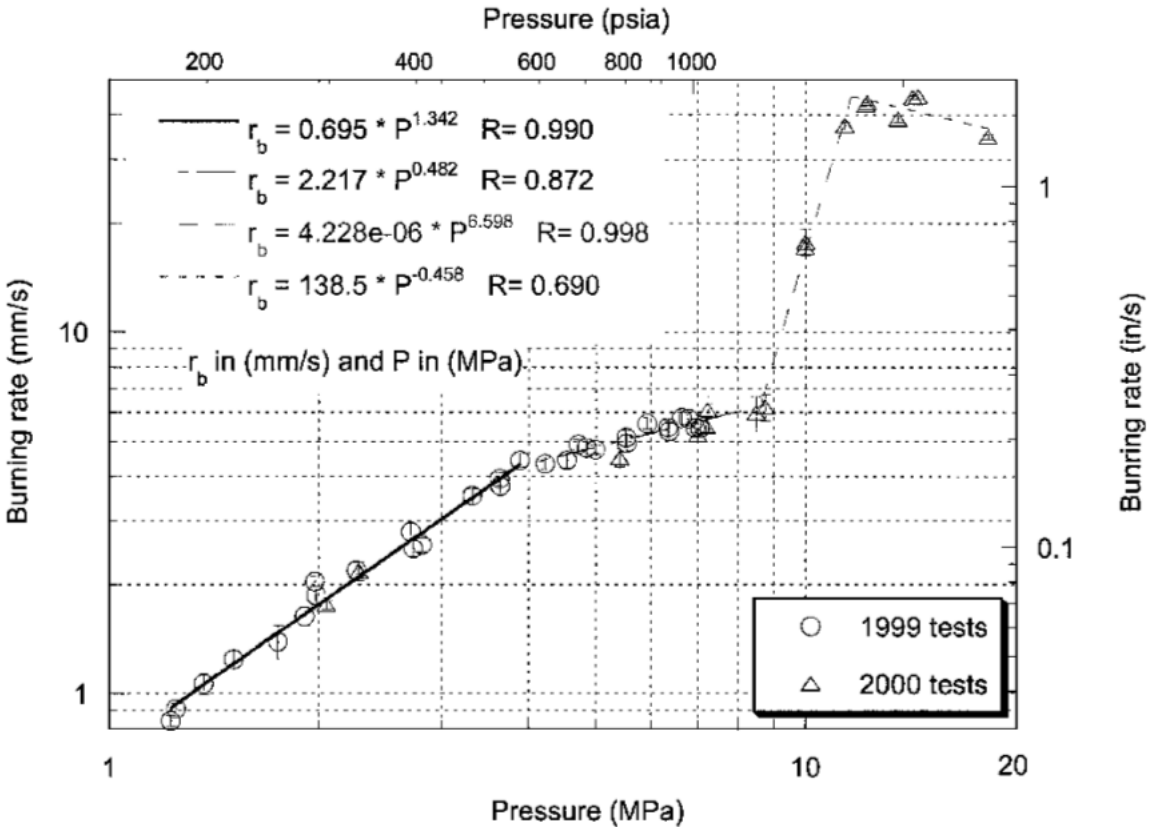

Fig. 2: Four distinct burn-rate regions for HANGLEY26 monopropellant. [7]

Chang [18] took things farther by performing additional experiments on HAN269, a propellant formulation of HAN-methanol that is nearly identical to the one studied in this research. Ranging from 0.74 to 6.4 MPa, HAN-methanol samples were combusted in the same

LPSB as Chang and Kuo's previous study. Reported were 5 separate burning regimes, with one being a potential discontinuity. Figure 3 shows Chang's findings.

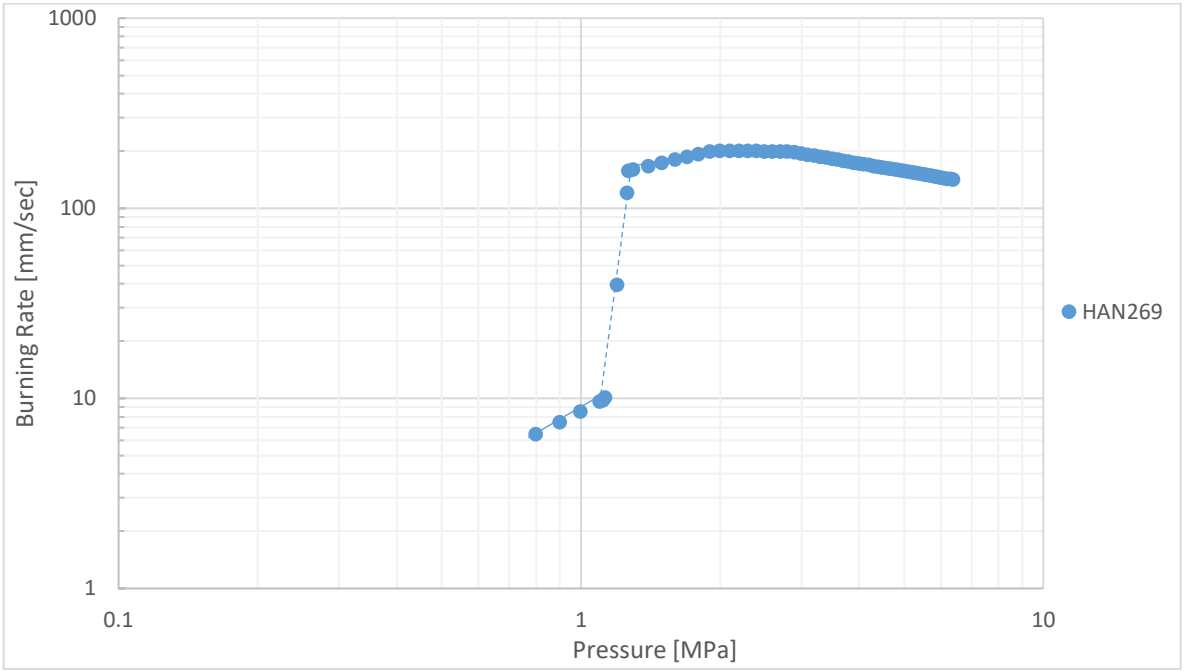

Fig. 3: There are five burning regimes, although the last three are subtle [18].

Another notable experiment is that by Connell [17], who performed an investigation into the burning rates of 13 Molar (M) HAN and HAN269, the same propellant formulation of HAN-water and again a very similar formulation of HAN-methanol that are the subject of this thesis. Connell utilized a very similar setup to Chang and Kuo, with a pressurized optical strand burner. In the experiment, 13M HAN and HAN269 combustion was observed via high-speed camera at pressures ranging from 1 MPa to 30 MPa. Further, Connell also added 1% Nitrocellulose (NC) to additional samples of HAN269 for comparison. Rather interestingly, Connell recorded at least five distinct burning regimes for HAN269, compared to two for 13M HAN and only a single regime for HAN269 with 1% NC added. Compared to Chang, Connell agreed with the first

regime for HAN269, but then adds an additional three on top of Chang's research. Figure 4 illustrates Connell's findings and the multiple burn regimes of the propellants.

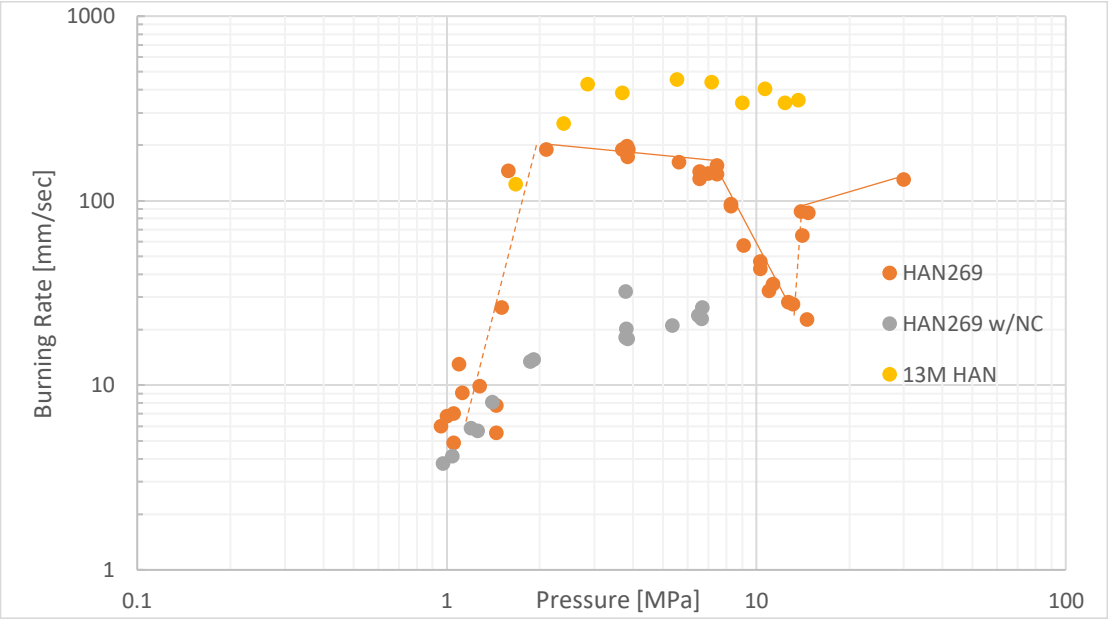

Fig. 4: Erratic burning behavior of HAN propellants from Connell [17].

It is worth noting that Connell's and Chang's experiments with HAN269 illustrate the unpredictable nature of HAN-based monopropellants. Such unpredictability is a paramount motivation for obtaining further data of these ionic propellants, so that the combustion behaviors as functions of pressure can be better understood.

2.3 Previous Usage of UHPOC

The Ultra-High-Pressure Optical Chamber (UHPOC) is a technology that presents new opportunities for the study of rocket and gun propellants. Previous methods for recording burn rates at high-pressure, such as the closed-bomb [1,3,4], have no way of observing flame

progression from combustion tests. This lack of flame-progression data means that these techniques rely on assumptions and models to back-solve for burn rate [3]. Therefore, optical combustion chambers are desirable for their ability to record data directly and validate models or produce more accurate ones. Additionally, optical recording of burn rates allows for an accuracy limited only by the resolution of the recording equipment, which generally results in less error than non-optical techniques [1,3,4]. The UHPOC allows for visual observation of combustion phenomena in excess of 300 MPa [3].

The UHPOC has been used for several recent pressure-dependent burn-rate experiments at the High-Pressure Combustion Lab. The chamber was initially validated with a standard solid propellant (JA2) to determine the accuracy of the process. Once the chamber's accuracy had been confirmed, Derk et al. [3,4] performed two notable experiments with nitromethane—a monopropellant notable for its erratic burning behavior at varying pressures. In both experiments, nitromethane was placed inside a glass tube and ignited inside the UHPOC. The flame propagation was recorded by highspeed camera.

In the first experiment, data was collected from 3.6 – 25.7 MPa. Between 3.6 – 18.2 MPa, the burning nitromethane showed a laminar flame surface. The burn-rate vs. pressure slope for this region was linear (on a log-log scale), in agreement with previous studies. However, at pressures greater than 18.2 MPa, the Dirk et al.'s experiment recorded a sharp increase in burn-rate. In addition, the slope for the burn-rate vs. pressure plot transitioned from linear to a non-linear. The region encompassing this transition from linear to non-linear burn-rate when is illustrated in Figure 5. The UHPOC data from this experiment was noted as differing significantly from previously published data in the transition region around 18 MPa [4]

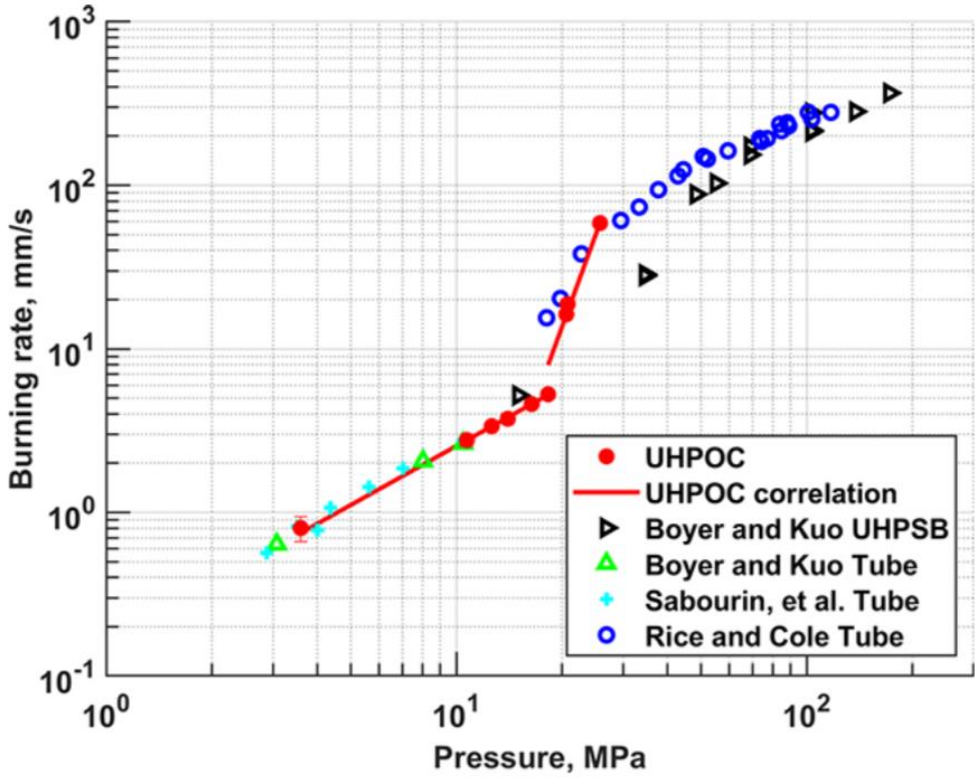

Fig. 5: UHPOC nitromethane burn-rate data shows sharp increase in burn rate followed by a non-linear region [4].

The second notable experiment with Nitromethane by Derk et. al [4] explored distinct combustion sample dimensions to observe the resulting effects on burn rate. The combustion of nitromethane in tubes of inner diameters ranging from 0.5 – 14 mm was tested at pressures between 3 and 75 MPa in the UHPOC. After 18 MPa, Dirk et al. notes a stark difference in burn rate across tube diameters. The difference is described generally as an increase in burn-rate with an increase in tube diameter, which is attributed to the change in turbulence scales, which correlate to tube diameter. The change in turbulence scale affects the burning surface area, which affects the burning rate. Figure 6 shows the UHPOC burn-rate vs. pressure data of nitromethane

with varying combustion tube diameters.

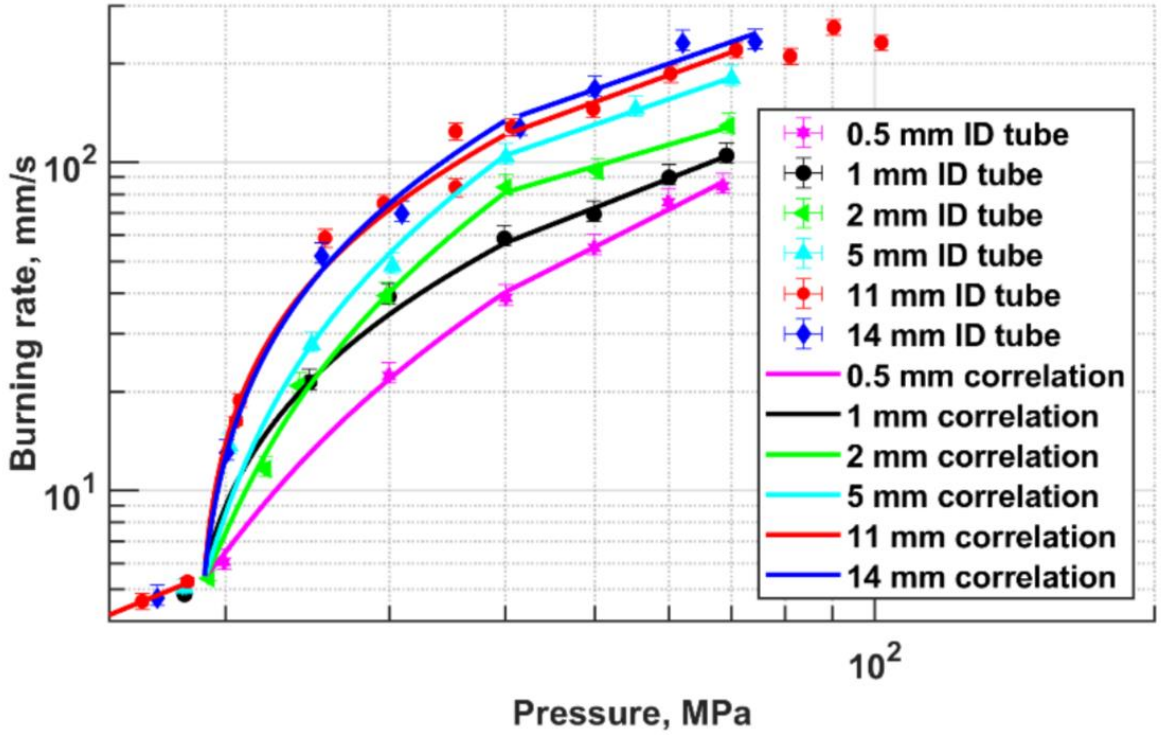

Fig. 6: Nitromethane burning rates from the UHPOC [4]

2.4. Gaps in Literature

Although many ionic monopropellants have been studies extensively, there are still questions that remain unanswered. For example, there is still little knowledge on how HAN formulation affects burn-rate as a function of pressure, nor is it known which component in the monopropellant causes the greatest variation in burn rate [7]. Klein [5] speculated that the structure of ammonium salts present during combustion are the cause for major burn-rate variations in HAN-based monopropellants, but admits that methods for predicting the behavior are flawed, because the empirical data he collected differed significantly from his predictions. In

addition to a lack of total understanding, there is also insufficient data on more modern ionic monopropellants at high pressures. McBratney and Vanderhoff [1] managed to record a variety of HAN-based monopropellants at high pressures, but many of these propellants have fallen out of favor with the propulsion community [10]. Moreover, modern formulations such as those studied by Chang [18] and Connell [17] show erratic burning behaviors. Although data recorded at extreme pressures is not directly applicable to today's rocket technology, it is necessary to record. Data for ionic monopropellants (like HAN-based monopropellants) at such pressures could exaggerate important behaviors and make them easier to identify and characterize. Therefore, more data and observations from ionic monopropellants are required to address these issues.

Chapter 3

Experimental Setup

3.1 The UHPOC

The UHPOC remains largely unchanged from Derk et al.'s [3,4] experiments for the purposes of this research. The chamber consists of a large, 4340 steel cylindrical section with an internal volume of 12 liters. This sizable volume allows for an accurate assumption of constant pressure around the test sample. Figure 7 shows the UHPOC as it stands in the test facility, while Figure 8 illustrates the manufacturer's drawing of the chamber cross-section. On the sides of the main body are two window sections that allow for viewing and lighting of the sample inside the chamber. Although the chamber is theoretically rated for a maximum working pressure in excess of 300 MPa, the real working pressure is dependent on the material of the windows that are installed on the chamber. With the fused quarts windows that were installed during this research, the chamber was previously recorded achieving a maximum pressure of 103 MPa before window failure [16].

Fig. 7: The UHPOC

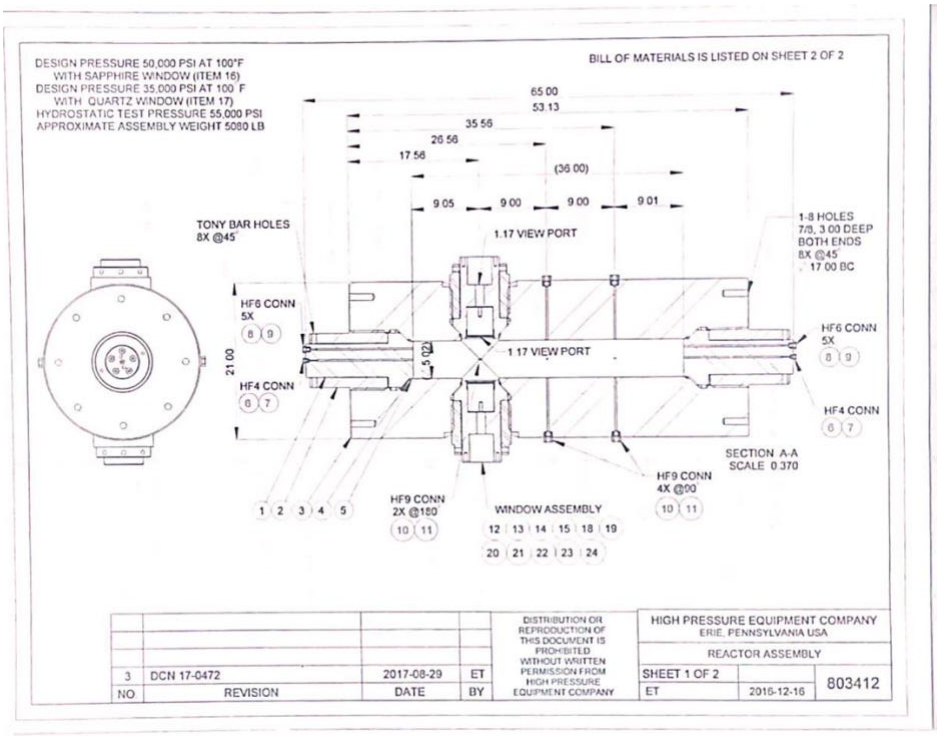

Fig. 8: The chamber consists of a volume, two windows, and a bottom end.

3.1.1 Plumbing

The plumbing for the UHPOC consists of high-pressure stainless-steel tubing that delivers a working gas of nitrogen into the main chamber. The nitrogen, being designated "< 2ppm moisture", is stored in a bank of four tanks at approximately 3000 psi. After the chamber has been fully sealed, the nitrogen can be fed to a Hydro-Pac Li'l Critter gas compressor (rated for 310 MP) to further pressurize the chamber beyond the bottle pressure. The compressor, being water cooled, requires a constant flow of 1-2 gpm from the building's water plumbing. The majority of this process is controlled with a series of variable needle and pneumatic isolation valves. The former regulates the gas flow rate into and out of the chamber, while the ladder toggle the gas inlet and exit. Figure 9 displays the plumbing layout of the UHPOC.

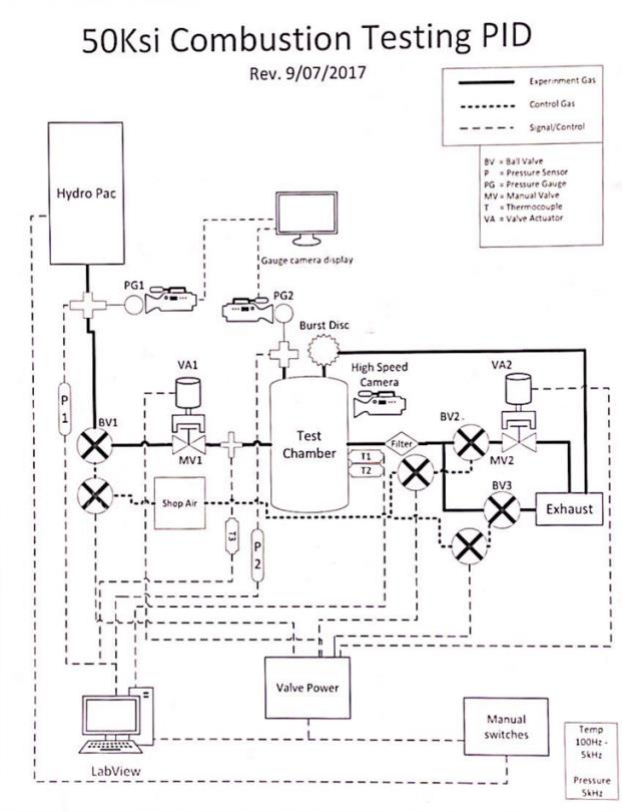

Fig. 9: Along with the high-pressure plumbing, there are low-pressure control lines.

In addition to the automated needle and isolation valves, there are 7 manually-operated valves that are open or closed by the chamber operator before and after each test. These consist of a valve to open the nitrogen supply bank, two valves for the high-pressure system, one valve for the low-pressure system, two exhaust valves, and a low-pressure release valve.

3.1.2 Control

The UHPOC plumbing can be controlled either by an analogue control panel or by a LabView computer program. Both methods can control the same chamber operations and are in place for redundancy, in case the other becomes unresponsive. Figure 10 and Figure 11 show the analogue and digital control interfaces, respectively. The control system has toggles for the isolation valves, switches for the isolation valves, and several displays for chamber pressure (a digital one, then two screens showing a CCTV feed of analogue gauges inside the chamber room). Although both of the control systems are considered redundant, the analogue control panel is the “master”, because it is the only one capable of switching control to the other system with a toggle. During normal operation, the analogue control panel is used for the chamber pressure management, while the LabView program is used to record the pressure-versus-time data for the chamber during a test.

Fig. 10: The LED lights on the panel serve as status indicators

Fig. 11: The digital setup is modeled after the analogue one.

3.1.3 Data Acquisition

The UHPOC data collection system consists of two main parts: LabView program, which monitors Omega PX91N1-50KS5T pressure sensors through a National Instruments USB-6361 data acquisition system, and the Phantom v310 high-speed camera, which records the sample combustion through the associated software. Figure 12 details the camera setup, with its blast-proof container and mirror to observe the chamber windows. By nature of the National Instruments DAQ, additional measurement functionality can be added easily in if needed for future experiments.

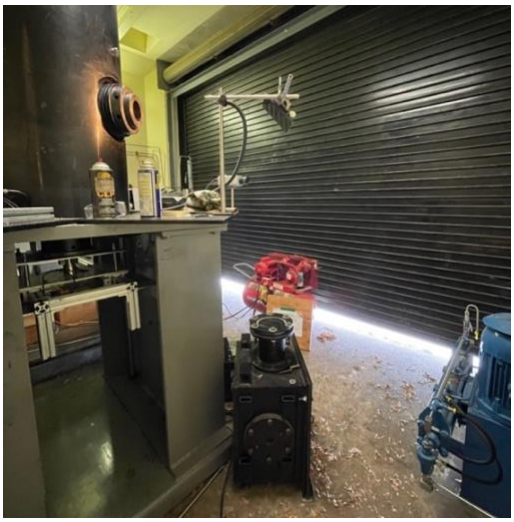

Fig. 12: The camera picks up a reflected image from the mirror.

3.1.4 Ad Hoc Modifications

This thesis proposes the investigation of two versions of HAN-based monopropellants. In addition, the testing procedure for any given propellant on the UHPOC is a time-consuming process. As such, it would be economical to test both propellant samples at the same time. Therefore, a double strand burner (as opposed to the currently-installed single-tube model) might be an effective way to reduce overall testing efficiency. Such a strand burner was designed be a direct bolt-on fit into the UHPOC hardware, and can be seen in Figure 13.

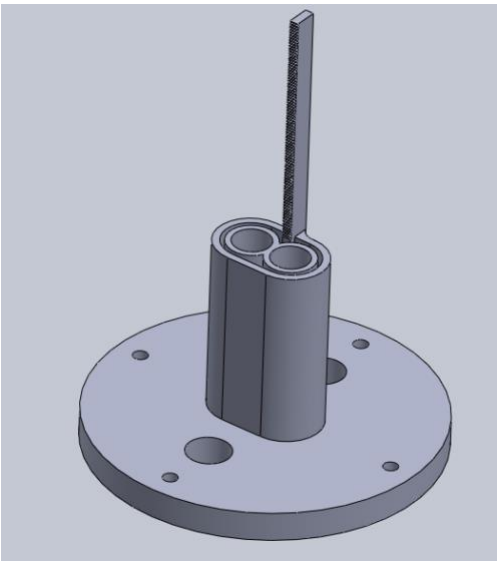

Fig. 13: The proposed dual strand burner, with two slots for individual tubes.

Beyond the ability to hold two sample tubes at once, the double strand burner features a center-mounted custom ruler marked in 1 mm increments. Also, at the base, there are two large passthroughs that allow for electronic clearance and ease of wiring. Surrounding the dual tube holders is a secondary wall that supports the ruler and has vent holes at the bottom. This entire apparatus was designed to be easily 3D printed with no supports. There are a few considerations

to make when 3D printing the double strand burner, chiefly material. The strand burner must be able to withstand extreme pressure changes as well as have excellent chemical resistance. The natural choices are nylon and polypropylene, which are both inexpensive and easily printable. Nylon is significantly stronger than polypropylene, but not as chemically resistant or mechanically resilient. Prototypes could be made with both of these materials and tested to determine which is best for this application.

3.2 Sample Preparation

This experiment utilized two different solutions of HAN and compared the two propellant's behavior at the same pressures. The formulations are as follows: 13 Molar (M) HAN solution, and HAN-methanol propellant that is very close in formulation to HAN269. The 13M HAN solution is approximately 83 wt. % HAN and 17 wt. % water, and as such, is referred to as HAN-water from this point on for clarity. The HAN-methanol solution is approximately 70 wt. % HAN and 15 wt. % methanol (MeOH).

Both the HAN-water and HAN-methanol solutions were tested in 10.6mm ID glass tubes. However, because of the energetic nature of the combustion of these species, the tubes exploded during initial tests. A simple remedy of wrapping the tube with clear packaging tape proved successful in fixing this problem. Subsequently, pre-prepared HAN-water or HAN-methanol was transferred to a taped tube. The filled tub was then placed in the strand-holder assembly. To complete the sample preparation, NOSOL solid ignitor propellant was threaded onto a segment of conductive nichrome wire. The nichrome and NOSOL assembly was placed in the copper alligator clips above the strand holder assembly, with the NOSOL dipping into the HAN sample

tube. With these steps complete, the HAN sample is ready to be combusted via the NOSOL/nichrome once the strand assembly is installed into the main chamber. See Figure 14 for a prepared sample in the strand assembly.

Fig. 14: The sample sits in the strand-holder with the NOSOL/nichrome ignitor [16].

Chapter 4

Procedure

4.1 Sample Loading Procedure

Once the sample tubes were transferred to the strand burner, the next step was to install the so-called “bottom end” assembly into the chamber. The bottom end is essentially a very large set-screw, with access ports for wires to run the internal electronics, such as the ignition system. The strand burner assembly is mounted to the top of the bottom end, which when installed positions it in perfect view of the UHPOC’s windows.

Because of the bottom end assembly’s weight, it requires a raising-platform system powered by an electric winch to lift into the bottom of the UHPOC. The raising-platform is easily unbalanced and as such, the operator must use his or her hands to steady the bottom end assembly as it is lifted into the chamber. Once the bottom end assembly is correctly positioned and lifted, the operator must screw the assembly into the chamber by hand with the aid of a long steel rod that slots into purpose-drilled holes in the bottom end. This process is very difficult and required a great deal of strength from the operator. Figure 15 shows the bottom end assembly before installation, while Figure 16 shows the bottom end assembly after installation, resting on the raising-platform.

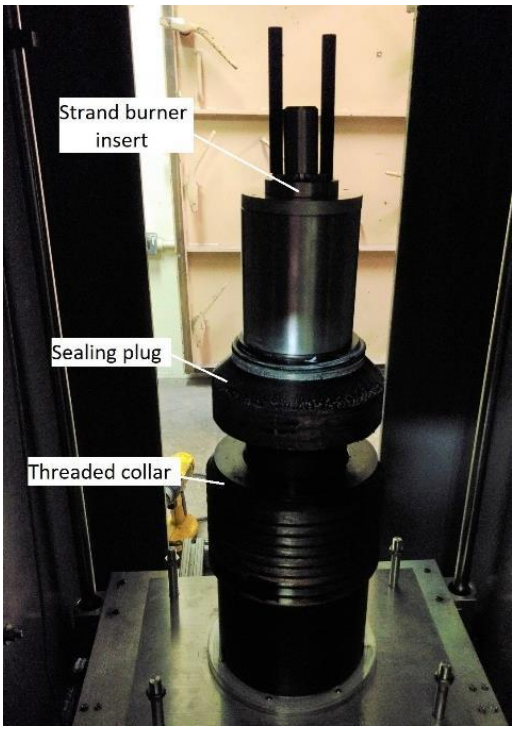

Fig. 15: Bottom end assembly with labeled components [16]

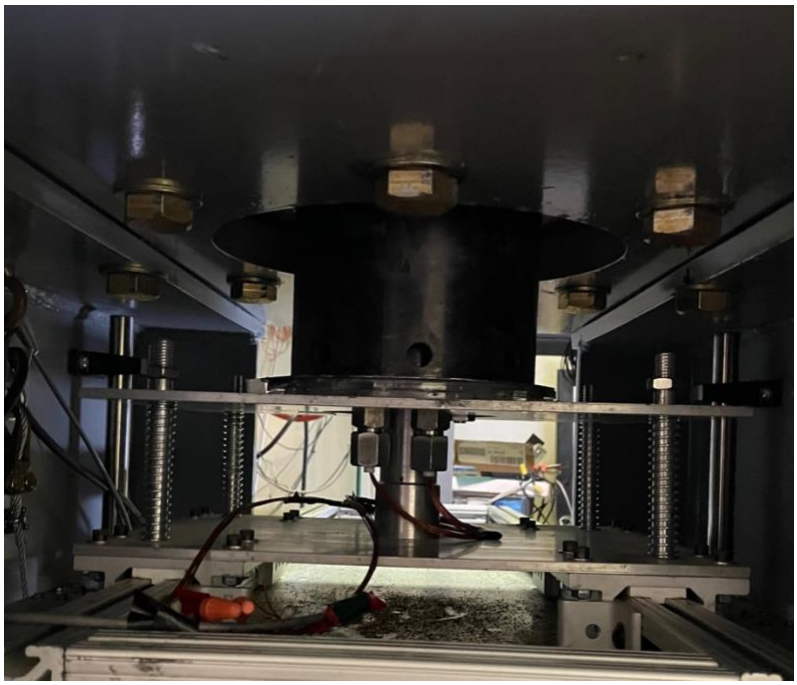

Fig. 16: Installed bottom end assembly, resting on the raising platform.

4.2 Chamber Pressurization Procedure

The UHPOC pressurization is a very long process. On the official operating procedure (listed in Appendix A), there are in excess of 50 steps to safely operate the machine. Some of these steps are relatively quick, but other steps can take over an hour. A regular day of testing during the course of this research would be in excess of 6 hours from start to finish to combust a single sample.

The procedure is preceded by the sample preparation steps discussed in subchapter 3.2, then the loading of the bottom end described in subchapter 4.1. After the performance of these prior processes, the pressurization of the UHPOC can begin. First, the control panels are turned on and verified. Next, the low-pressure buffer system is turned on with a small air compressor. Once the low-pressure system is activated, various exhaust valves are opened to allow proper depressurization of the chamber once testing is over. The camera system is then activated, and set to “ruler-capture” settings.

There is a metric ruler next to the sample tube on the strand burner that is visible to the camera, so that the flame progression can be correctly scaled and measured with the software package ImageJ in the data analysis. The “ruler-capture” settings for the camera are a simple 24 frames-per-second (FPS) and 10,000 millisecond exposure time, so that the ruler is clearly visible next to the test tube for post-processing. A short video is captured of the ruler, and then the camera is changed to “burn-capture” settings, or 2500 FPS and 400 millisecond exposure. The “burn-capture” settings are used to record the combustion in slow motion and are compared to the “ruler” video for scaling in the analysis. From this point, the water coolant pipe for the

HydroPac compressor is opened, and the final preparations are made for the chamber pressurization.

To begin pressurization, the nitrogen bottles are opened to allow gas flow into the chamber. The nitrogen bottles are opened in pairs: a pair of “low-pressure” bottles, and then a pair of “high-pressure” bottles. The “low-pressure” bottles are simply older bottles that may have less pressure than the “high-pressure” bottles. Once the chamber pressure has equalized with the low-pressure bottles, the high-pressure bottles are opened to further increase the pressure. As the pressure levels off a second time, the HydroPac compressor is turned on to reach the desired pressure in the UHPOC. This step can take upwards of an hour to complete depending on the pressure.

4.3 Burn and Unloading Procedure

After reaching the desired chamber, the experiment can be performed. The NOSOL/nichrome ignition wire as defined in subchapter 3.2 is connected to a VARIAC variable power supply which functions as the ignitor. An appropriate voltage is selected on the VARIAC, and then the operator starts recording the sample. The operator then flips the ignition switch on the control panel, then ends the recording as soon as the flame has propagated through the strand burner. After saving the burn video and then the LabView output, the chamber is ready for depressurization.

Despite taking over an hour to pressurize, the depressurization process takes only minutes. Once the chamber is depressurized, the operator repeats the same tasks in reverse that

he or she did to load the sample. The used sample can be inspected after the bottom end is removed.

HAN decomposition leads to products that, if left on the chamber surfaces, can cause serious corrosion. Thus, after the final steps in the official operating procedure are complete, the operator must clean the inside of the chamber after a HAN test. The UHPOC cleaning process added to the operating procedure specifically to address the corrosion caused by HAN tests. The chamber is cleaned in three steps using rags attached to a long rod: first, a general wipe to get most of the liquid; second, a methanol wipe; third, a coating of gun lubricant to keep further corrosion from occurring.

Chapter 5

Results and Analysis

5.1 Data Analysis Methodology

The experiment data captured by the LabView and camera systems was compiled and analyzed into average burning rates of the propellant and qualitative combustion characteristics. The videos were mathematically processed with ImageJ, a software that can plot distance versus time when given a known measurement. As mentioned in subchapter 4.2, two videos are taken of a single sample. The first video is taken with the front of the sample lit inside the chamber to expose the ruler next to the strand burner. This initial "ruler" video is used to set the correct scaling within ImageJ. The second video captures the burn of the sample. However, in this second video, the sample is backlit so as the ruler is no longer visible. Thus, this is called the "burn" video, and is the primary subject of analysis.

To analyze the videos within ImageJ, CINE-raw files are uploaded to the program. First, the ruler video is used to set the scale. The user draws a line on top of the ruler (which is in millimeters) to a visually countable distance. The "set-scale" command is then used, which determines the "pixels per millimeter" after the user inputs the counted distance. The ruler video has now fulfilled its purpose, and the user inputs the determined scaling into the burn video. Utilizing the "multi-point" command, the user marks the top center of the flame profile and then forwards to another point in time to mark another point. The time between each point on the video is arbitrary, because the burning rate for any given sample at any given pressure is linear

and will follow the same trend no matter the 'delta-t' between data points. Once 15 points are recorded, the "measure" tool outputs a table of y-position versus time of the flame surface. It is worth noting that Derk [16] states that the error from human-selected points on the flame surface is less than 2%, and thus this method is a suitable avenue of analysis.

After ImageJ produces the table, the user copies it into Microsoft Excel and makes a plot of y-distance versus time. A line of best fit can be generated—the slope of which is the burning rate of the propellant at that pressure. The Excel plots for each individual sample can be found in Appendix B.

5.2 Burning Rate of 13M HAN

13M HAN, or simply referred to as HAN-water in this case, was tested at pressures ranging from 30 to 70 MPa. The burning rate of the HAN-water tested over the course of the experiment followed a decreasing trend, as if a continuation of the second burn regime defined by Connell [17]. For each subsequent pressure increment, the burn-rate decreased with exception of 50 MPa, where the burn-rate increased very slightly over the 40 MPa point. The following 70 MPa data point showed a sharp decrease in burning rate. Figure 17 illustrates the data from this research along with Connell's findings for the same propellant.

The linear correlation for this data, or the St. Robert's Law equation, was found to be $r_b = 66723(P\ [MPa])^{-1.711}$. It is worth noting that there are not many comparisons to make between these findings and the literature, as there are little sources that combust 13M HAN above 10 or 20 MPa. The closest is perhaps McBratney and Vanderhoff [1], who found that the behavior of gelled 9.1M HAN did not have any obvious slope breaks or decreases in burning rate

over the same pressures of 30-70 MPa. However, given the unpredictable nature of HAN-based propellants, these findings may not mean anything at all when compared to 13M HAN.

What is most interesting is the relatively large negative exponent of the correlation. When negative exponents are displayed for HAN-water, they tend not to be very large in magnitude, with a few exceptions. Chang [18] noted a negative pressure exponent region with HAN269, but the exponent was very small.

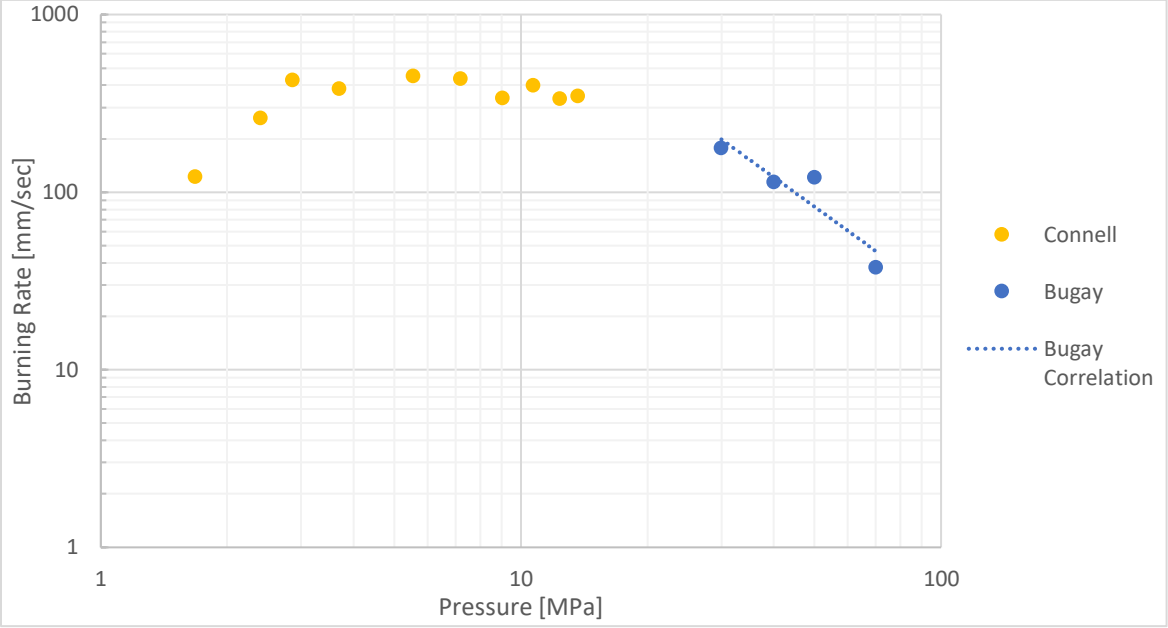

Fig. 17: The burning rate regime above 30 MPa shows a clear downward regression.

5.3 Burning Rate of HAN-methanol

The HAN-methanol was also tested at pressures ranging from 30 to 70 MPa. Similar to HAN-water, the burning rate of the HAN-methanol followed a decreasing trend, albeit more extreme. Starting at 30 MPa, each data point decreased in burning rate with increasing pressure.

The correlation was found to follow the equation $r_b = (1 * 10^6)(P\ [MPa])^{-2.506}$. This correlation demonstrates an even greater and more extreme pressure exponent than was found with HAN-water. Similar to HAN-water, the HAN-methanol exhibited a sharp decrease in burning rate for the 70 MPa data point. Figure 18 details the findings for HAN-methanol superimposed on Chang's [18] and Connell's [17] data for HAN269. Since the formulations of HAN269 and the HAN-methanol used in this research are very nearly identical, they will be approximated as the same for ease of discussion.

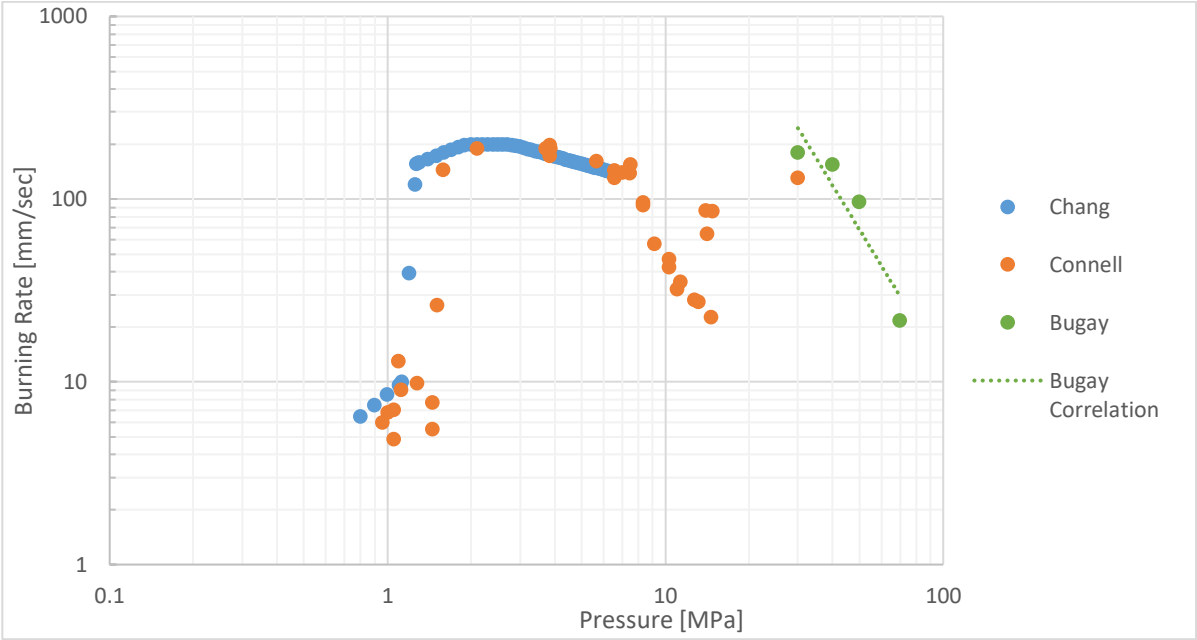

Fig. 18: Although a similar trend to HAN-water, the HAN-methanol exhibits a sharper decline.

Several sources from the literature serve for noteworthy comparison, such as the experiments by Chang and Connell. Although not reaching the same pressure levels, these two sources to illustrate the different burn regimes of HAN-methanol. While the HAN-water results seemed to more or less continue the same downward trend of Connell's experiment, the HAN-

methanol results show a completely new behavior, and an extreme one at that. Assuming that the new data is only one burn regime (it may indeed be several, but more tests are required to confirm the trends), the pressure exponent of -2.506 is unlike most anything else in the literature. That being said, the general trend of the HAN-methanol exhibits similar traits to that of HAN-water in the same pressure region. Both propellants have a negative slope with a pressure exponent around -2. Likewise, the actual values of the burn rates themselves are similar between the two propellants. For reference, Table 2 lists the burning rates of HAN-water and HAN-methanol across the tested pressures.

Table 2: The similar burning rates of 13M HAN and HAN-methanol.

Pressure	Burn rate of 13M HAN	Burn rate of HAN-methanol
30 MPa	177.08 mm/sec	179.05 mm/sec
40 MPa	114.15 mm/sec	154.56 mm/sec
50 MPa	121.38 mm/sec	96.485 mm/sec
70 MPa	37.673 mm/sec	21.673 mm/sec

The relative similarity of burn rates and trends between HAN-water and HAN-methanol in the tested pressure range would suggest that HAN is the dominant reactant. For some unknown reason, the methanol seems to “take a back seat” to the HAN in this pressure range and minimally contribute to the speed of the reaction. This is contrasted to the pressure ranges studied by Connell, where the HAN-methanol had significantly lower burn rates at the same pressure as HAN-water. The data suggests that over the pressure ranges in Connell’s experiment, methanol has a much more significant influence over the burning rate than in the new pressure

range studied by this thesis. Figure 19 presents a cohesive plot of all HAN-water and HAN-methanol data for comparison.

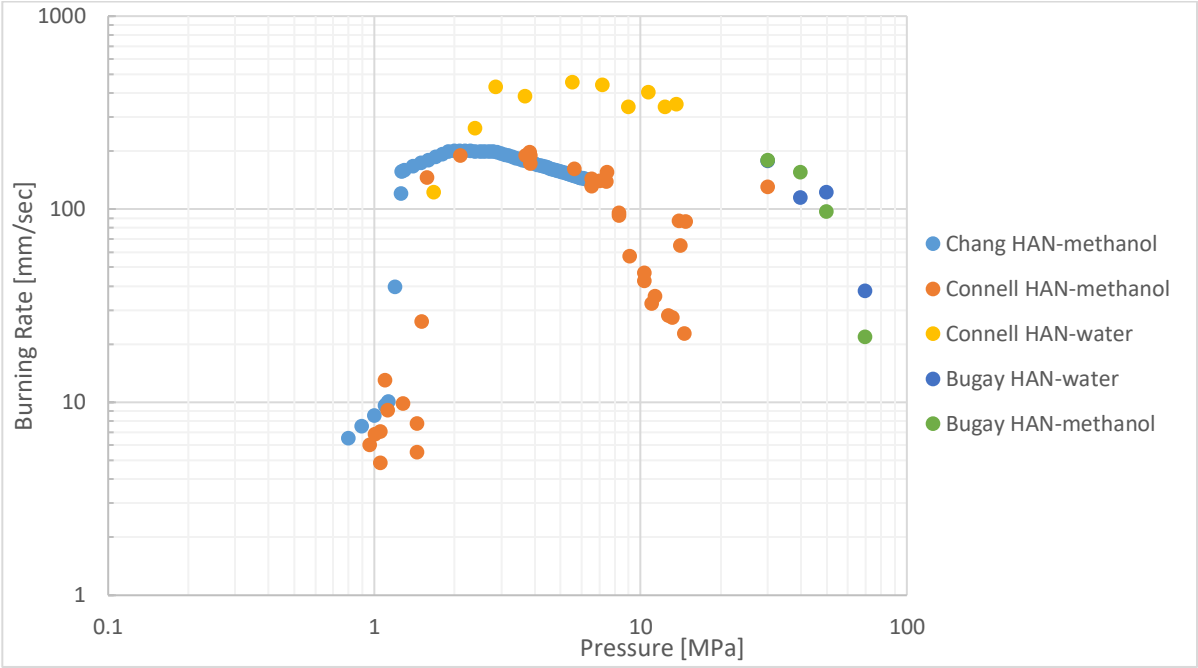

Fig. 19: Comprehensive comparison for all formulations.

5.4 Flame Surface

As a part of this analysis, CEA computer code was run as an enthalpy-pressure problem for both HAN-water and HAN-methanol. The code was run for each of the pressures tested as a part of the experiment, with the purpose of discerning if flame temperature had a significant influence on the combustion reaction. The CEA temperature results as a function of pressure are recorded in Table 3. For additional reference, the CEA output code is recorded in Appendix C. It should be noted that the CEA code assumes ideal gas equations of state and does not consider real gas behaviors.

Table 3: Flame temperatures from CEA demonstrate little variance.

Pressure	13M HAN Flame Temp	HAN-methanol Flame Temp
30 MPa	725.72 K	2177.6 K
40 MPa	719.62 K	2178.59 K
50 MPa	718.14 K	2179.23 K
70 MPa	717.11 K	2180.11 K

Notice how despite changing pressures drastically, the calculated flame temperature has negligible variance. Especially given the relatively large volume of the propellant samples, it is unlikely that a maximum temperature difference of 8 Kelvin between the tests made any significant difference to the combustion process. However, what is interesting is the large variance of flame color, shape and behavior that the samples exhibited despite theoretically having insignificant temperature change. The HAN-methanol samples go from a turbulent orange flame, to a very turbulent orange flame, to a dark opaque gas, then to a white flame with very little turbulence. Figure 20 shows the flame surface progression for each tested pressure. The 70 MPa flame was particularly unexpected. Most HAN-based monopropellants when photographed exhibit large instabilities and turbulence, as is seen with the 30 and 40 MPa samples. By contrast, the 70 MPa sample shows an almost laminar flame with very small bubbles on the flame surface. In addition, the white color is also inconsistent with HAN-methanol at lower pressures.

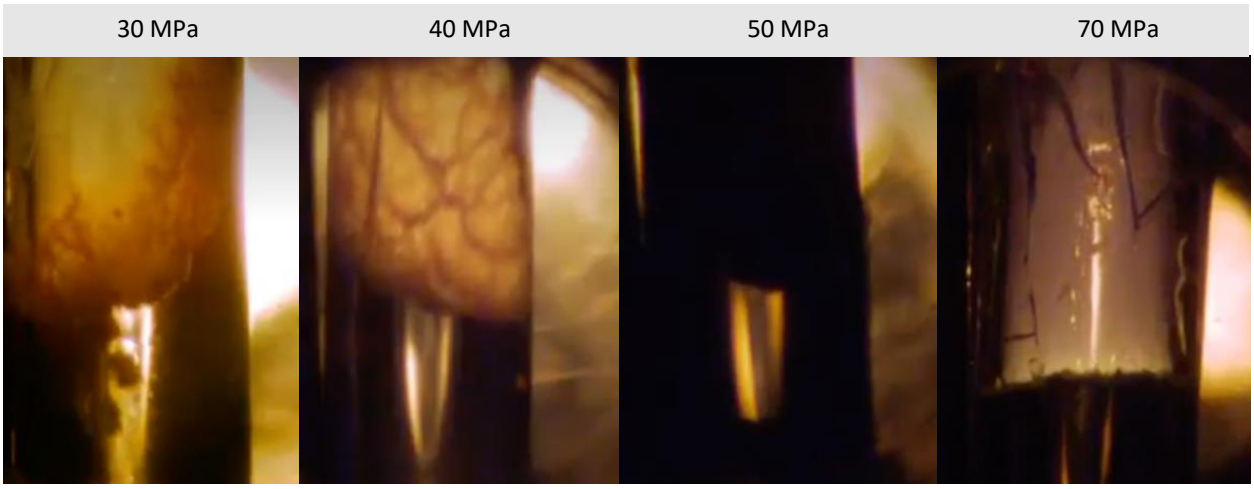

Fig. 20: Strand burner images show amazing changes in the flame structure from HAN-methanol samples.

There are a couple of concerns when addressing the HAN-methanol flame structures that were recorded in this research. First and foremost, the 70 MPa sample of HAN-methanol was a newly-mixed batch of propellant, unlike the previous tests. Although the same formulation, it is still a potential inconsistency, because there was not time for sufficient performance validation before the completion of this thesis. The second concern is the 50 MPa sample, which was left in the chamber for a day before the test could take place. Connell [17] partially addresses this issue, having concluded that HAN-methanol does not evaporate or noticeably change composition when exposed to the atmosphere for a few days. Still, particles from inside the chamber could have contaminated the sample. Some relief to these concerns may be found in the comparison of HAN-methanol to the HAN-water burn rates, which are in marginal agreement at all tested pressures.

In contrast to the vibrant behavior of HAN-methanol, the HAN-water samples exhibited only a single type of flame: dark and opaque. Given the nature of these flames, it is hard to determine what mechanisms (turbulence, instabilities, etc.) might be occurring on the flame surface. Figure 21 illustrates the flames of HAN-water at the different pressures tested. This flame appearance is consistent with Chang [18] who found that HAN could often produce brown opaque flames.

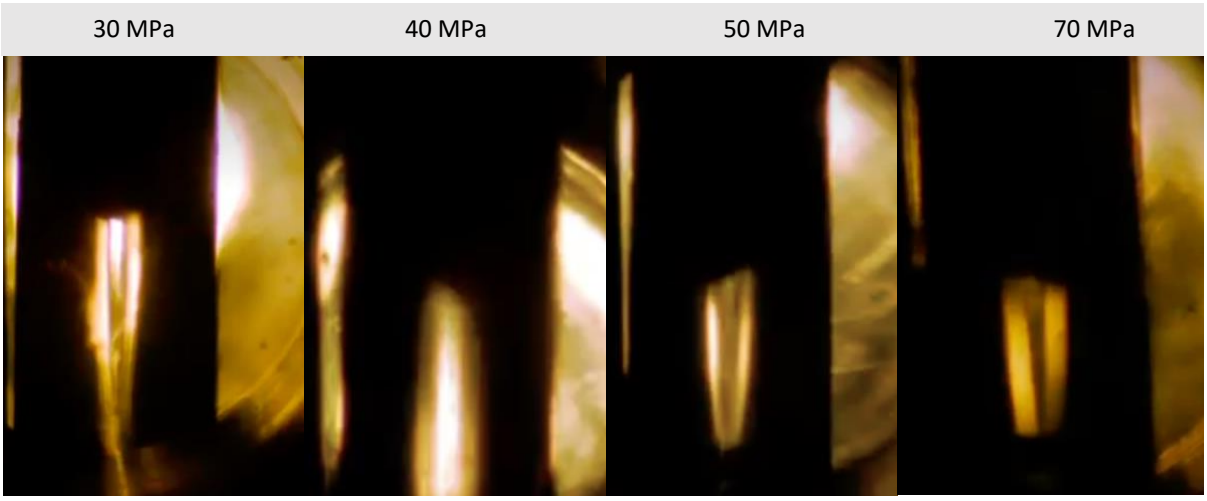

Fig. 21: Strand burner images show similar opaque flame structures from HAN-water samples.

The same sample concerns that existed for HAN-methanol do not exist for HAN-water, because none of the samples were left in the chamber overnight and all of the samples were taken from the same batch.

Chapter 6

Discussion and Conclusion

6.1 Interpretation and Takeaways

In this research, HAN-water and HAN-methanol samples were combusted via strand burner at high ambient pressures inside a unique pressure chamber, the UHPOC. To determine the burning rates of each sample, a Phantom high-speed camera was used to record optical data which was then analyzed with ImageJ and Microsoft Excel. In addition, flame temperature was calculated with CEA and compared to images of the flame surface of the propellants at each pressure. Finally, the results were compared to previous, lower-pressure studies of the same propellants.

It was shown that starting at 30 MPa and until 70 MPa that both HAN-water and HAN-methanol propellants dramatically decrease in burn rate. The negative pressure exponent of the St. Robert's Law correlation for both propellants is large compared to negative pressure exponent regions at lower pressures. This effect was more pronounced for the HAN-methanol than the HAN-water. Further, it can be hypothesized that the dominant molecule in the combustion process at these pressures is HAN, considering the similar burn rates and trends of HAN-methanol to that of HAN-water. The dominance of HAN in the tested pressure range is direct contrast to the behaviors of the two propellants at lower pressures, where it is evident that methanol has a much more profound influence over the burn rate.

Despite CEA calculations showing virtually identical flame temperatures across all tested pressures, the HAN-methanol samples showed drastically different flame colors, structures, and behaviors. 30 MPa and 40 MPa flames only differed by the amount of turbulence, while 50 MPa

and 70 MPa were completely different. The 50 MPa flame for HAN-methanol was more similar to all of the flames for HAN-water (dark and opaque), while the 70 MPa flame was white and the surface showed little turbulence. The mechanism for these flame changes is not yet known.

6.2 Recommendations for Future Work

This research gives insight to the behaviors of HAN-based monopropellants, as well as the influence of HAN itself over different propellant formulations. However, many questions are raised as a result of these findings. For example, perhaps the most pressing question is related to the flame structures seen from HAN-methanol. As previously mentioned, the mechanisms behind these changes are not known, and would require further analysis.

The scope of this research was impacted by the COVID-19 pandemic, and as such, requires additional validation. There are potential inconsistencies, such as a new batch of HAN-methanol, that could be addressed in future testing. More data could also be useful in confirming or disputing the results presented in this thesis.

Further, improvements to the UHPOC could be made to increase reliability and speed of operation. A protective coating on the inside of the chamber would significantly reduce problems caused by corrosion, and updating some of the electronics could lead to less failures. Additional nitrogen bottles, or potentially a higher-pressure nitrogen source would drastically decrease pressurization times. A new gas supply method, coupled with a double strand burner (similar to the one proposed in subchapter 3.1.5) would decrease test times and increase general productivity.

Appendix A

UHPOC Standard Operating Procedures

A.1 General Safety Procedures

1. Always wear appropriate PPE when entering the chamber or handling propellants.
2. Always wear safety goggles whenever any gas bottles are turned on
3. Limit the amount of propellant for any given experiment to the minimum amount needed.

   This minimizes the over pressurization risk.

4. Never enter the chamber when the system is pressurized.

   There are rare occasions when this is necessary – if so, consult with the lab manager to

   determine additional safety procedures that must be followed.

5. Visually inspect the plumbing and electrical systems weekly to look for any signs of wear

   or distress.

   Never inspect plumbing or wiring while the system is energized or pressurized.

6. Before any test, understand the hazards of the propellant and any combustion products.

   This knowledge is critical should an unexpected event occur.

A.2 Bottom end-closure installation

General note, do not let spring-loaded plate compress fully. Damage to the turntable and possibly the full assembly will result.

1. Prepare sample in strand burner
2. Slide end-closer assembly until it hits the stops on the horizontal rails.

3. Set/Verify the Variac for the winch to ~15%. This slows the lifting rate of the winch.
4. Begin lifting assembly – be aware that it will begin to tilt as soon as it is off of the ground.
5. Once the plug is near the opening, hold the assembly vertically to prevent it from being

   caught on the edge of the opening.

6. Continue raising the assembly until the threaded collar has contacted the opening and the springs are almost, but not fully, compressed.

7. Manually lift the threaded collar and rotate it until it catches in the threads of the opening.
8. Use a bar, inserted into the access holes on the collar, to screw the collar into the chamber.

   Do not insert the bar more than 1" into the holes at it will catch on the inner plug causing the sample to be rotated out of position. If the plug turns when the threaded collar turns, either hold the plug in place or add more anti-seize to lubricate it.
   As the springs decompress, the assembly will become harder to turn. After the springs have decompressed approximately half-way, lift the base plate more to take off some of the weight.

   Caution: when the threaded collar is about half-way screwed in, the lifting assembly will have the plug fully seated within the chamber. At this point, do not raise the lifter any more as it will break the lifting assembly. Continue screwing the collar in until it is fully installed. The last few rotations will be harder, but the assembly should still move smoothly.

A.3 Compressor Startup and Chamber Filling

1. Perform all pre-test data collection (Room temp, sample size, etc.)
2. Test that internal illumination is operational (if using)

3. Install sample per "Bottom end-Closure" installation SOP
4. Turn on power strip on bottom of control panel
5. Turn on master power to control panel
6. Turn on Red air compressor for control gas and let it pump up.
7. Turn off red compressor when it reaches ~100 psi. It has plenty of volume so doesn't need to run while testing.

8. Verify HV2 is open. This is the valve between the air compressor and the plumbing panel.
9. Set pressure levels on LabVIEW to read zero; begin monitoring pressure
10. Outside the test cell, close HV1, the isolation valve between the N2 source and the buffer bottle
11. Set the high-speed camera to use ruler-capture settings
12. Turn on the fiber light
13. Cover the camera and run the CSR process on the high-speed camera
14. If using polycarbonate windows:

    Open the upstream isolation valve
    Close downstream isolation valve and dump valve
    Pressurize chamber to ~200 psi using the green buffer bottle to spread out mineral oil and verify the scale is visible.

15. Once windows are verified, close the upstream isolation valve and open the green buffer bottle.
16. Verify sample is visible through window and through camera(s).
17. Verify all data-collection equipment is in place and operational
18. Verify hydraulic fluid level on compressor is full (above the temperature scale on the window)
19. Open the rolling metal door to the chamber by ~1 ft.

20. Turn on exterior warning light
21. Open both valves on outside of building for exhaust and relief valve plumbing
22. Turn on cooling water for compressor. Ensure flow rate is ~1-2 gal/min.
23. Close the door to the test cell
24. Verify 3-way valve on high-pressure system is closed to the test cell.
25. Open in-building vent (HV3) for high-pressure plumbing
26. Ensure valve between test cell and HPCL high-p plumbing is closed (HV4)
27. Open the source N2 bottles and verify you have enough gas for the test (compressor will not operate below 800 PSI)
28. Close the Downstream isolation valve and dump valve
29. Fully close (decrease) the downstream needle valve
30. Make sure the upstream needle valve is at least partially open. There is no "openness" indicator, so you if you are unsure, running it in the "increase" direction until it stops ensures it is fully open.

31. If not using polycarbonate windows, now pressurize the chamber to ~200 psi by opening the isolation valve.

32. Open dump valve to let the chamber evacuate to below 100 psi. This removes the air/moisture that was in the chamber prior to being sealed.

33. Open HV1 between the N2 bottles and the buffer bottle
34. Open the upstream isolation valve to begin filling the chamber
35. Wait for the chamber pressure to level off.
36. Turn on the breaker to power the gas compressor.

    The compressor does not turn off automatically, so this process must be monitored

37. Begin capturing high-speed video with a trigger set to capture all past data. Trigger the camera if a failure happens during pressurization.

38. Turn off the breaker to the compressor power once the desired pressure has been reached.

Target Pressure _____

39. Close the Upstream isolation valve.
40. Wait for the pressure to equalize in the system before beginning test.
41. Ensure all three isolation valves on the control panel are closed.
42. Close HV1 between N2 bottles and buffer bottle
43. Close the source N2 bottles

A.4 Test Execution procedures

1. Ensure door to test cell is fully closed
2. Turn on Variac and adjust to proper setting

   JA2 and Nitromethane use ~17-18 for most pressures.

   If testing below 2000 psi, try a lower setting such as 10-15.

3. Turn on internal illumination (if using)
4. Capture lit video of ruler and save to .mp4 format
5. Record chamber pressure
6. Change high-speed camera recording settings.
7. Start high-speed video capture
8. Start Labview data collection
9. Arm ignitor
10. Ignite

11. Trigger high-speed camera as soon as flame extinguishes
12. Turn off ignitor
13. Disarm ignitor
14. Stop data collection
15. Turn off internal illumination (if using)
16. Turn Variac off
17. Save burn video to .mp4 and .cine (RAW) format
18. Convert LabView data file from TDMS raw format.
19. Save data to thumb drive and move to the data repository on the main network

A.5 End of test procedures

1. Open the downstream isolation valve.
2. Open the downstream needle valve until gas begins to exit the chamber.

Do not open fully while at high pressures to limit the stress on the low-pressure exhaust

plumbing.

3. When chamber falls below 3000 psi and you can enter the room briefly using appropriate PPE and close the green buffer bottle.
4. Open the Upstream isolation valve. Also open the upstream needle valve if it was closed before the test.
5. Wait until the chamber pressure and compressor pressure has been fully released. Can open the dump valve to speed things up if necessary.
6. Once the pressure has been released, open the dump valve (assuming it wasn't open already from step 5).
7. Close the upstream and downstream isolation valves
8. Close the downstream needle valve.
9. Let test cell air out for a few minutes after venting completes because there is a LOT of nitrogen in the area.
10. Turn off exterior warning light
11. Collect any post test data needed (window deflection, etc.)
12. Clean inside and outside of windows with soft gauze and a mild soap and water solution
13. Clean sample holder in strand burner
14. Inspect windows for damage or fatigue

If testing is done for the day

1. Close both valves on the exterior of building for exhaust and relief valve plumbing
2. Close vent valve (HV3) inside building for high-pressure plumbing
3. Turn off cooling water to the compressor
4. Verify fluid hydraulic levels on compressor are full
5. Shut down the master on the control panel
6. Turn off the power strip on the bottom of the control panel
7. Close the rolling metal door to the chamber.

A.6 Bottom end-closure removal

General note, do not let spring-loaded plate compress fully. Damage to the turntable and possibly the full assembly will result.

1. Raise lifting mechanism until the center round support is fully seated on the inner plug.

   The springs on the movable support plate will be slightly compressed.

2. Use a bar, inserted into the access holes on the collar, to unscrew the collar from the

   chamber.
   Do not insert the bar more than 1" into the holes at it will catch on the inner plug causing it to be rotated along with the collar. If the plug turns when the threaded collar turns, either hold the plug in place or add more anti-seize to lubricate it.
   As the springs get close to full compression, lower the lifter to give the springs more travel room. Lower a little bit at a time, corresponding to each round of unscrewing. When the collar fully unscrews, it will drop onto the movable plate and you want to limit the amount of distance it drops.

3. Continue lowering the lifter until the widest part of the plug is about to exit the opening. Hold the assembly vertically while lowering the lifter until the plug is fully out of the opening. Allow the mechanism to fully settle in whatever orientation it prefers. Failure to hold the assembly will cause it to tilt dramatically after exiting the opening, causing damage to the sealing surface of the plug.
4. Lower the lifter until all four support legs are on the floor. Don't continue running the winch past this point to prevent the cable from coming off of the rollers.

A.7 Compressor Maintenance

General Notes:

- During the winter, and any other time it is expected to get below freezing outside, keep the

heater running in the test cell. The compressor is water cooled, and bad things will happen if the water in the compressor freezes.

- If testing is not occurring, run the compressor for at least 30 minutes every week. It can be

  run safely with the gas bottles turned off.

- If the compressor is shutdown or stored for longer than two weeks, it needs to be protected

  from corrosion.

  - The best way to do this is to run the compressor using lightweight oil or other

corrosion inhibiting fluid. This will leave a film that will protect the barrel bores

and other parts that may corrode.

- When the compressor is restarted, all the internal parts should be cleaned unless

the protective fluids compatible with the compressed gas system requirements.

- The compressor should be protected from extreme changes in temperature that could cause

condensation to occur.

Yearly Maintenance:
The end of the spring semester / beginning of summer (April-May) is the timeframe for yearly compressor maintenance

- The strainer and hydraulic reservoir should be cleaned yearly.
- The hydraulic oil should be replaced yearly. Compatible oils are listed in the compressor

  manual.

A.8 Loss of System Control

Blowout or venting of combustion products to room:

1. Notify lab manager and PI immediately.
2. Do not enter room until it can be deemed safe.

127 3. If either the propellant or products are toxic and/or harmful, follow lab procedures for

handling and cleanup.

Loss of system control:
The UHPOC system is designed to fail to a safe state should all control be lost to the system. However, should control be lost:

1. Notify the lab manager immediately.
2. Do not enter room until it can be deemed safe.
3. If unable to manipulate and observe system via one of the control systems (hardware or

   software), use the control switch on the hardware panel to switch control to the other system. These systems are independent and redundant, so they should be able to take over control for each other to bring the system back to a safe state.

4. If neither control system is able to manipulate the system, cut all electrical power to the hardware control panel. This will turn off all valves in the chamber, causing the system to fail to an open state.
5. In the unlikely event the dump valve is stuck, cutting power to the panel will not help. You can attempt to retain control of the system by restarting the hardware control panel.
6. If all control attempts have failed and the system is still pressurized, work with the lab manager to call in specialized safety personnel.

Unable to determine system state although appear to still have control:

1. Notify the lab manager immediately.
2. Do not enter room until it can be deemed safe.

3. If you are unable to see source and chamber pressure through either the analog gauges or digital readouts, open the downstream isolation and/or dump valves to vent chamber. The evacuation of gasses is easy to hear, so use that as a guide to whether the camber is venting.

4. Wait a minimum of 30 minutes after opening vents before entering room. The valves can sometimes freeze up with long depressurization events from high pressures, so this wait time ensures that the chamber is fully depressurized and not just slowed down due to a stuck valve.

Appendix B

Excel Plots for Burning Rate

B.1 HAN-water Plots

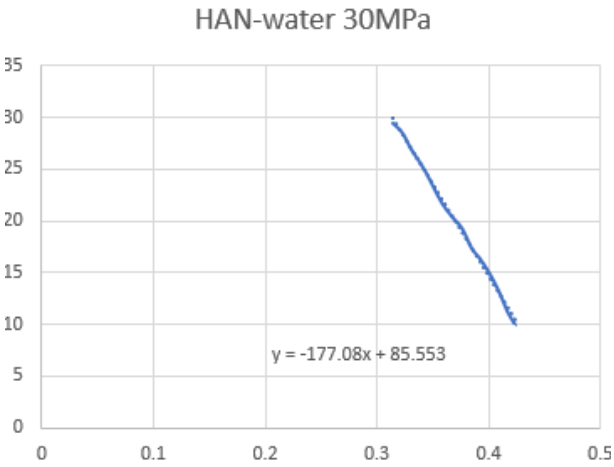

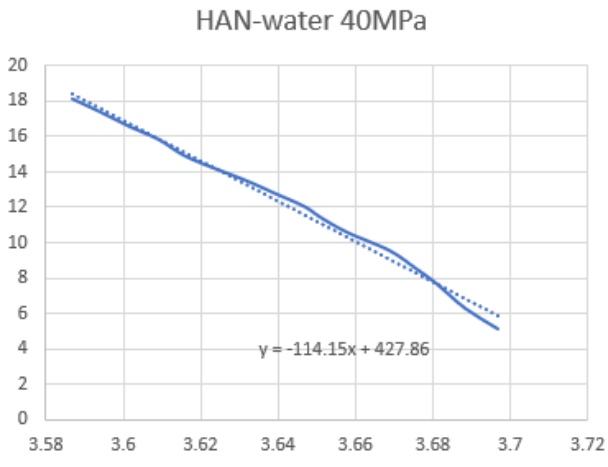

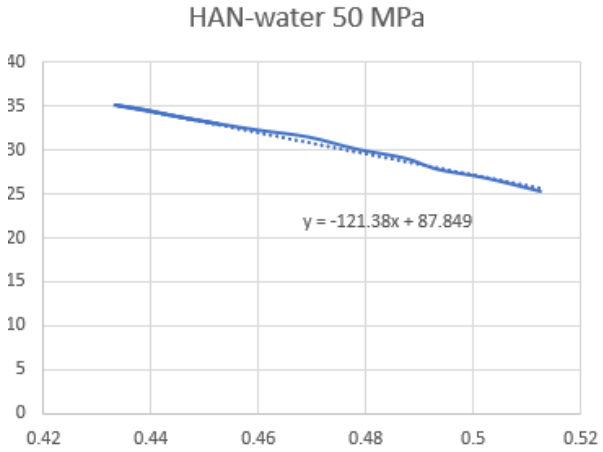

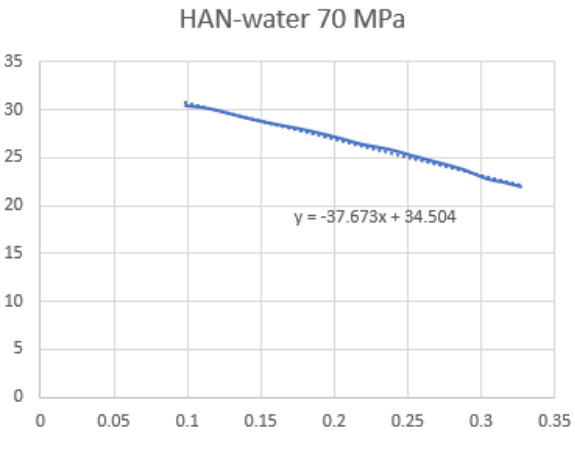

B.2 HAN-methanol Plots

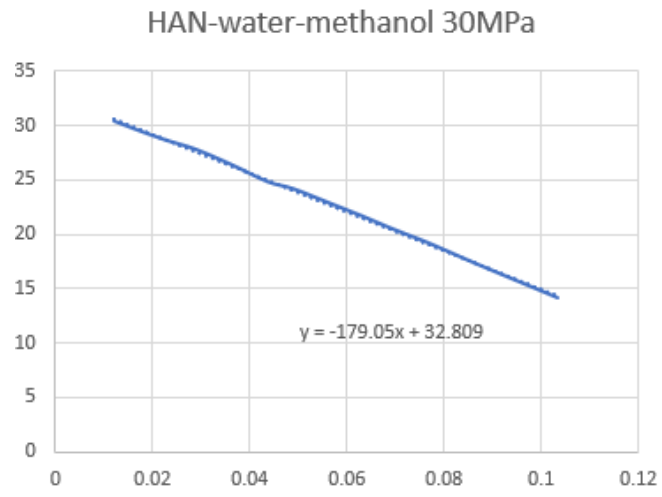

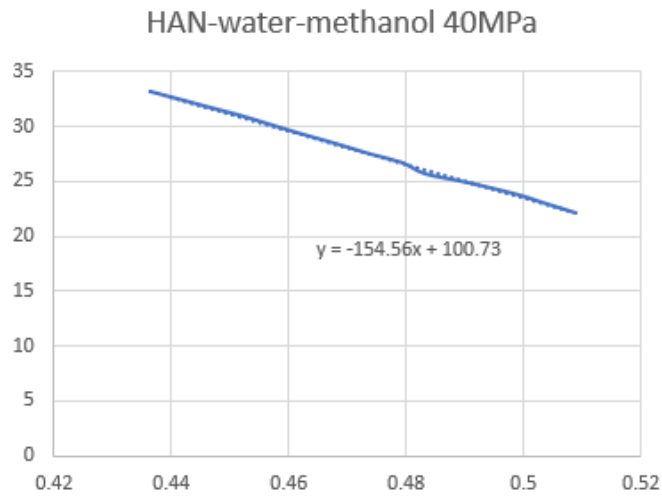

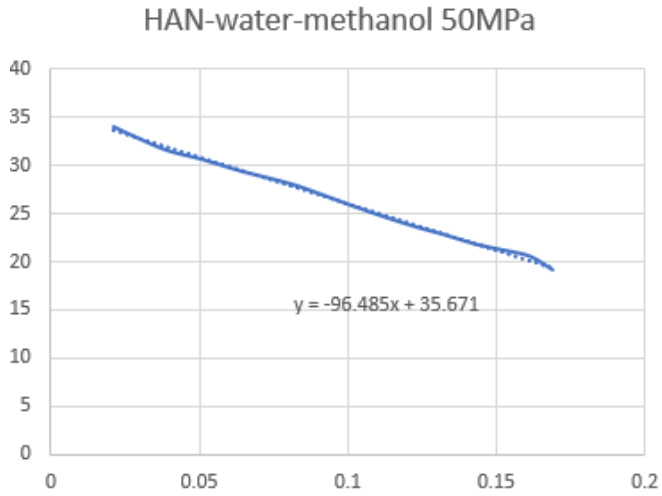

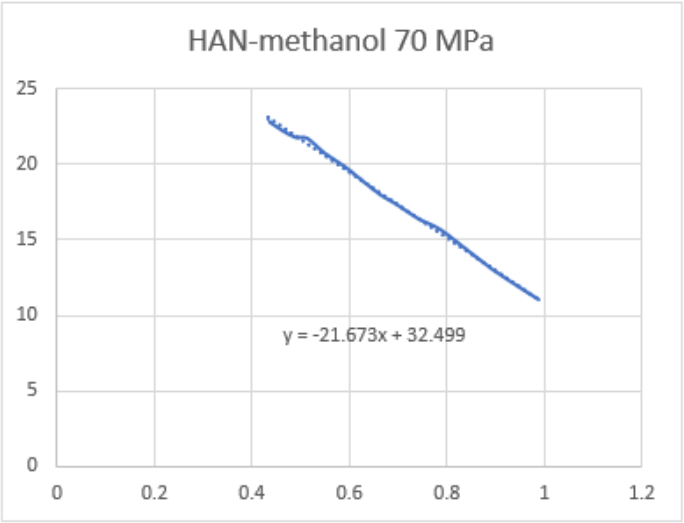

Appendix C

CEA Output Codes

C.1 HAN-water CEA Output Code

```
******************************************************************************

      NASA-GLENN CHEMICAL EQUILIBRIUM PROGRAM CEA2, MAY 21, 2004
              BY  BONNIE MCBRIDE AND SANFORD GORDON
    REFS: NASA RP-1311, PART I, 1994 AND NASA RP-1311, PART II, 1996

******************************************************************************



problem
     hp   p,bar=300,400,500,700,  t,k=2000
react
  name=H2O(L) wt=.18  t,k=298
  name=HAN  wt=.82  t,k=298
    h,kj/mol=-344.76  H 4 N 2 O 4
insert
  H2O(L)
end

OPTIONS: TP=F  HP=T  SP=F  TV=F  UV=F  SV=F  DETN=F  SHOCK=F  REFL=F  INCD=F
 RKT=F  FROZ=F  EQL=F  IONS=F  SIUNIT=T  DEBUGF=F  SHKDBG=F  DETDBG=F  TRNS
PT=F

T,K =  2000.0000

TRACE= 0.00E+00  S/R= 0.000000E+00  H/R= 0.000000E+00  U/R= 0.000000E+00

P,BAR =   300.000000   400.000000   500.000000   700.000000

   REACTANT         WT.FRAC   (ENERGY/R),K   TEMP,K  DENSITY
      EXPLODED FORMULA
N: H2O(L)          0.180000  -0.343786E+05   298.00  0.0000
       H  2.00000  O  1.00000
N: HAN             0.820000  -0.414649E+05   298.00  0.0000
       H  4.00000  N  2.00000  O  4.00000
```

SPECIES BEING CONSIDERED IN THIS SYSTEM
(CONDENSED PHASE MAY HAVE NAME LISTED SEVERAL TIMES)
LAST thermo.inp UPDATE: 10/22/02

g 6/97 *H	g10/01 HNO	tpis89 HNO2
g 5/99 HNO3	g 4/02 HO2	tpis78 *H2
g 8/89 H2O	g 6/99 H2O2	g 5/97 *N
g 4/99 *NH	g 3/01 NH2	tpis89 NH3
tpis89 NH2OH	tpis89 *NO	g 4/99 NO2
j12/64 NO3	tpis78 *N2	g 5/99 N2H2
tpis89 NH2NO2	g 4/99 N2H4	g 4/99 N2O
g 4/99 N2O3	tpis89 N2O4	g 4/99 N2O5
tpis89 N3	g 4/99 N3H	g 5/97 *O
g 4/02 *OH	tpis89 *O2	g 8/01 O3
g11/99 H2O(cr)	g 8/01 H2O(L)	g 8/01 H2O(L)
H2O(L) INSERTED		

O/F = 0.000000

	EFFECTIVE FUEL	EFFECTIVE OXIDANT	MIXTURE
ENTHALPY	h(2)/R	h(1)/R	h0/R
(KG-MOL)(K)/KG	-0.69751596E+03	0.00000000E+00	-0.69751596E+03

KG-FORM.WT./KG	bi(2)	bi(1)	b0i
*H	0.54134492E-01	0.00000000E+00	0.54134492E-01
*O	0.44142973E-01	0.00000000E+00	0.44142973E-01
*N	0.17075728E-01	0.00000000E+00	0.17075728E-01

POINT	ITN	T	H	O	N
1	16	725.717	-24.127	-10.742	-9.910
2	10	719.622	-24.412	-10.475	-9.644
3	7	718.140	-24.537	-10.302	-9.470
4	7	717.114	-24.679	-10.070	-9.239

THERMODYNAMIC EQUILIBRIUM COMBUSTION PROPERTIES AT ASSIGNED

PRESSURES

CASE =

	REACTANT	WT FRACTION (SEE NOTE)	ENERGY KJ/KG-MOL	TEMP K
NAME	H2O(L)	0.1800000	-285841.390	298.000
NAME	HAN	0.8200000	-344760.000	298.000

O/F= 0.00000 %FUEL= 0.000000 R,EQ.RATIO= 0.613172 PHI,EQ.RATIO= 0.000000

THERMODYNAMIC PROPERTIES

P, BAR	300.00	400.00	500.00	700.00
T, K	725.72	719.62	718.14	717.11
RHO, KG/CU M	1.4121 2	2.3813 2	3.3633 2	5.3302 2
H, KJ/KG	-5799.50	-5799.50	-5799.50	-5799.50
U, KJ/KG	-6011.95	-5967.48	-5948.17	-5930.83
G, KJ/KG	-11763.2	-11659.3	-11612.1	-11557.0
S, KJ/(KG)(K)	8.2176	8.1428	8.0939	8.0287
M, (1/n)	28.402	35.620	40.164	45.402
MW, MOL WT	22.654	22.654	22.654	22.654
(dLV/dLP)t	-2.06192	-1.64411	-1.45811	-1.28990
(dLV/dLT)p	-1.2265	0.1787	0.5020	0.7218
Cp, KJ/(KG)(K)	10.7148	14.3268	16.2635	18.0616
GAMMAs	0.4948	0.6084	0.6873	0.7784
SON VEL,M/SEC	324.2	319.7	319.7	319.7

MOLE FRACTIONS

H2O	0.41078	0.24916	0.17721	0.11214
NO2	0.00000	0.00000	0.00000	0.00001
*N2	0.19341	0.19341	0.19341	0.19341
*O2	0.19341	0.19341	0.19341	0.19341
H2O(L)	0.20240	0.36402	0.43597	0.50104

* THERMODYNAMIC PROPERTIES FITTED TO 20000.K

PRODUCTS WHICH WERE CONSIDERED BUT WHOSE MOLE FRACTIONS WERE LESS THAN 5.000000E-06 FOR ALL ASSIGNED CONDITIONS

*H	HNO	HNO2	HNO3	HO2
*H2	H2O2	*N	*NH	NH2
NH3	NH2OH	*NO	NO3	N2H2
NH2NO2	N2H4	N2O	N2O3	N2O4
N2O5	N3	N3H	*O	*OH
O3	H2O(cr)			

NOTE. WEIGHT FRACTION OF FUEL IN TOTAL FUELS AND OF OXIDANT IN TOTAL OXIDANTS

C.2 HAN-methanol CEA Output Code

```
******************************************************************************

      NASA-GLENN CHEMICAL EQUILIBRIUM PROGRAM CEA2, MAY 21, 2004
            BY  BONNIE MCBRIDE AND SANFORD GORDON
    REFS: NASA RP-1311, PART I, 1994 AND NASA RP-1311, PART II, 1996

******************************************************************************



problem
   hp   p,bar=300,400,500,700,  t,k=2000
react
  name=H2O(L) wt=.15  t,k=298
  name=CH3OH(L) wt=.15  t,k=298
  name=HAN  wt=.70  t,k=298
   h,kj/mol=-344.76  H 4 N 2 O 4
end


OPTIONS: TP=F  HP=T  SP=F  TV=F  UV=F  SV=F  DETN=F  SHOCK=F  REFL=F  INCD=F
 RKT=F  FROZ=F  EQL=F  IONS=F  SIUNIT=T  DEBUGF=F  SHKDBG=F  DETDBG=F  TRNS
PT=F


T,K =  2000.0000


TRACE= 0.00E+00  S/R= 0.000000E+00  H/R= 0.000000E+00  U/R= 0.000000E+00


P,BAR =   300.000000   400.000000   500.000000   700.000000


   REACTANT         WT.FRAC   (ENERGY/R),K   TEMP,K  DENSITY
      EXPLODED FORMULA
 N: H2O(L)          0.150000  -0.343786E+05   298.00  0.0000
       H  2.00000  O  1.00000
 N: CH3OH(L)        0.150000  -0.287356E+05   298.00  0.0000
       C  1.00000  H  4.00000  O  1.00000
 N: HAN             0.700000  -0.414649E+05   298.00  0.0000
       H  4.00000  N  2.00000  O  4.00000
```

SPECIES BEING CONSIDERED IN THIS SYSTEM
(CONDENSED PHASE MAY HAVE NAME LISTED SEVERAL TIMES)
LAST thermo.inp UPDATE: 10/22/02

g 7/97 *C tpis79 *CH g 4/02 CH2
g 4/02 CH3 g11/00 CH2OH g 7/00 CH3O
g 8/99 CH4 g 7/00 CH3OH srd 01 CH3OOH
g 8/99 *CN g12/99 CNN tpis79 *CO
g 9/99 *CO2 tpis91 COOH tpis91 *C2
g 6/01 C2H g 1/91 C2H2,acetylene g 5/01 C2H2,vinylidene
g 4/02 CH2CO,ketene g 3/02 O(CH)2O srd 01 HO(CO)2OH
g 7/01 C2H3,vinyl g 9/00 CH3CN g 6/96 CH3CO,acetyl
g 1/00 C2H4 g 8/88 C2H4O,ethylen-o g 8/88 CH3CHO,ethanal
g 6/00 CH3COOH srd 01 OHCH2COOH g 7/00 C2H5
g 7/00 C2H6 g 8/88 CH3N2CH3 g 8/88 C2H5OH
g 7/00 CH3OCH3 srd 01 CH3O2CH3 g 7/00 CCN
tpis91 CNC srd 01 OCCN tpis79 C2N2
g 8/00 C2O tpis79 *C3 n 4/98 C3H3,1-propynl
n 4/98 C3H3,2-propynl g 2/00 C3H4,allene g 1/00 C3H4,propyne
g 5/90 C3H4,cyclo- g 3/01 C3H5,allyl g 2/00 C3H6,propylene
g 1/00 C3H6,cyclo- g 6/01 C3H6O,propylox g 6/97 C3H6O,acetone
g 1/02 C3H6O,propanal g 7/01 C3H7,n-propyl g 9/85 C3H7,i-propyl
g 2/00 C3H8 g 2/00 C3H8O,1propanol g 2/00 C3H8O,2propanol
srd 01 CNCOCN g 7/88 C3O2 g tpis *C4
g 7/01 C4H2,butadiyne g 8/00 C4H4,1,3-cyclo- n10/92 C4H6,butadiene
n10/93 C4H6,1butyne n10/93 C4H6,2butyne g 8/00 C4H6,cyclo-
n 4/88 C4H8,1-butene n 4/88 C4H8,cis2-buten n 4/88 C4H8,tr2-butene
n 4/88 C4H8,isobutene g 8/00 C4H8,cyclo- g10/00 (CH3COOH)2
n10/84 C4H9,n-butyl n10/84 C4H9,i-butyl g 1/93 C4H9,s-butyl
g 1/93 C4H9,t-butyl g12/00 C4H10,n-butane g 8/00 C4H10,isobutane
g 6/01 C4N2 g 8/00 *C5 g 5/90 C5H6,1,3cyclo-
g 1/93 C5H8,cyclo- n 4/87 C5H10,1-pentene g 2/01 C5H10,cyclo-
n10/84 C5H11,pentyl g 1/93 C5H11,t-pentyl n10/85 C5H12,n-pentane
n10/85 C5H12,i-pentane n10/85 CH3C(CH3)2CH3 g 2/93 C6H2
g11/00 C6H5,phenyl g 8/00 C6H5O,phenoxy g 8/00 C6H6
g 8/00 C6H5OH,phenol g 1/93 C6H10,cyclo- n 4/87 C6H12,1-hexene
g 6/90 C6H12,cyclo- n10/83 C6H13,n-hexyl g 6/01 C6H14,n-hexane
g 7/01 C7H7,benzyl g 1/93 C7H8 g12/00 C7H8O,cresol-mx
n 4/87 C7H14,1-heptene n10/83 C7H15,n-heptyl n10/85 C7H16,n-heptane
n10/85 C7H16,2-methylh n 4/89 C8H8,styrene n10/86 C8H10,ethylbenz
n 4/87 C8H16,1-octene n10/83 C8H17,n-octyl n 4/85 C8H18,n-octane
n 4/85 C8H18,isooctane n10/83 C9H19,n-nonyl g 3/01 C10H8,naphthale
n10/83 C10H21,n-decyl g 8/00 C12H9,o-bipheny g 8/00 C12H10,biphenyl
g 6/97 *H g 6/01 HCN g 1/01 HCO
tpis89 HCCN g 6/01 HCCO g 6/01 HNC
g 7/00 HNCO g10/01 HNO tpis89 HNO2

g 5/99 HNO3 g 4/02 HO2 tpis78 *H2
g 5/01 HCHO,formaldehy g 6/01 HCOOH g 8/89 H2O
g 6/99 H2O2 g 6/01 (HCOOH)2 g 5/97 *N
g 6/01 NCO g 4/99 *NH g 3/01 NH2
tpis89 NH3 tpis89 NH2OH tpis89 *NO
g 4/99 NO2 j12/64 NO3 tpis78 *N2
g 6/01 NCN g 5/99 N2H2 tpis89 NH2NO2
g 4/99 N2H4 g 4/99 N2O g 4/99 N2O3
tpis89 N2O4 g 4/99 N2O5 tpis89 N3
g 4/99 N3H g 5/97 *O g 4/02 *OH
tpis89 *O2 g 8/01 O3 n 4/83 C(gr)
n 4/83 C(gr) n 4/83 C(gr) g11/99 H2O(cr)
g 8/01 H2O(L) g 8/01 H2O(L)

O/F = 0.000000

	EFFECTIVE FUEL	EFFECTIVE OXIDANT	MIXTURE
ENTHALPY	h(2)/R	h(1)/R	h0/R
(KG-MOL)(K)/KG	-0.72298085E+03	0.00000000E+00	-0.72298085E+03

KG-FORM.WT./KG	bi(2)	bi(1)	b0i
*H	0.64531716E-01	0.00000000E+00	0.64531716E-01
*O	0.42161323E-01	0.00000000E+00	0.42161323E-01
*C	0.46813762E-02	0.00000000E+00	0.46813762E-02
*N	0.14576841E-01	0.00000000E+00	0.14576841E-01

POINT	ITN	T	H	O	C	N
1	21	2177.665	-10.778	-14.271	-21.919	-11.671
2	3	2178.585	-10.702	-14.131	-21.904	-11.528
3	2	2179.233	-10.643	-14.022	-21.893	-11.416
4	3	2180.110	-10.555	-13.858	-21.878	-11.249

THERMODYNAMIC EQUILIBRIUM COMBUSTION PROPERTIES AT ASSIGNED

PRESSURES

CASE =

REACTANT		WT FRACTION (SEE NOTE)	ENERGY KJ/KG-MOL	TEMP K
NAME	H2O(L)	0.1500000	-285841.390	298.000
NAME	CH3OH(L)	0.1500000	-238922.161	298.000
NAME	HAN	0.7000000	-344760.000	298.000

O/F= 0.00000 %FUEL= 0.000000 R,EQ.RATIO= 0.987365 PHI,EQ.RATIO= 0.000000

THERMODYNAMIC PROPERTIES

P, BAR	300.00	400.00	500.00	700.00
T, K	2177.66	2178.59	2179.23	2180.11
RHO, KG/CU M	3.7201 1	4.9585 1	6.1967 1	8.6725 1
H, KJ/KG	-6011.23	-6011.23	-6011.23	-6011.23
U, KJ/KG	-6817.66	-6817.93	-6818.12	-6818.38
G, KJ/KG	-28425.3	-28202.6	-28029.2	-27766.5
S, KJ/(KG)(K)	10.2927	10.1862	10.1035	9.9790

M, (1/n)	22.452	22.454	22.456	22.458
(dLV/dLP)t	-1.00033	-1.00029	-1.00027	-1.00024
(dLV/dLT)p	1.0100	1.0089	1.0082	1.0071
Cp, KJ/(KG)(K)	2.3916	2.3796	2.3712	2.3598
GAMMAs	1.1871	1.1878	1.1883	1.1889
SON VEL,M/SEC	978.4	978.9	979.2	979.6

MOLE FRACTIONS

*CO	0.00041	0.00036	0.00033	0.00028
*CO2	0.10470	0.10476	0.10480	0.10485
*H	0.00001	0.00001	0.00000	0.00000
HO2	0.00000	0.00000	0.00000	0.00001
*H2	0.00055	0.00048	0.00043	0.00037
H2O	0.72322	0.72340	0.72352	0.72369

*NO	0.00090	0.00090	0.00090	0.00089
NO2	0.00000	0.00000	0.00000	0.00001
*N2	0.16319	0.16321	0.16322	0.16323
*O	0.00001	0.00001	0.00001	0.00001
*OH	0.00133	0.00124	0.00118	0.00109
*O2	0.00567	0.00563	0.00560	0.00557

* THERMODYNAMIC PROPERTIES FITTED TO 20000.K

PRODUCTS WHICH WERE CONSIDERED BUT WHOSE MOLE FRACTIONS WERE LESS THAN 5.000000E-06 FOR ALL ASSIGNED CONDITIONS

*C *CH CH2 CH3 CH2OH
CH3O CH4 CH3OH CH3OOH *CN
CNN COOH *C2 C2H C2H2,acetylene
C2H2,vinylidene CH2CO,ketene O(CH)2O HO(CO)2OH C2H3,vinyl
CH3CN CH3CO,acetyl C2H4 C2H4O,ethylen-o CH3CHO,ethanal
CH3COOH OHCH2COOH C2H5 C2H6 CH3N2CH3
C2H5OH CH3OCH3 CH3O2CH3 CCN CNC
OCCN C2N2 C2O *C3 C3H3,1-propynl
C3H3,2-propynl C3H4,allene C3H4,propyne C3H4,cyclo- C3H5,allyl
C3H6,propylene C3H6,cyclo- C3H6O,propylox C3H6O,acetone C3H6O,propanal
C3H7,n-propyl C3H7,i-propyl C3H8 C3H8O,1propanol C3H8O,2propanol
CNCOCN C3O2 *C4 C4H2,butadiyne C4H4,1,3-cyclo-
C4H6,butadiene C4H6,1butyne C4H6,2butyne C4H6,cyclo- C4H8,1-butene
C4H8,cis2-buten C4H8,tr2-butene C4H8,isobutene C4H8,cyclo- (CH3COOH)2
C4H9,n-butyl C4H9,i-butyl C4H9,s-butyl C4H9,t-butyl C4H10,n-butane
C4H10,isobutane C4N2 *C5 C5H6,1,3cyclo- C5H8,cyclo-
C5H10,1-pentene C5H10,cyclo- C5H11,pentyl C5H11,t-pentyl C5H12,n-pentane
C5H12,i-pentane CH3C(CH3)2CH3 C6H2 C6H5,phenyl C6H5O,phenoxy
C6H6 C6H5OH,phenol C6H10,cyclo- C6H12,1-hexene C6H12,cyclo-
C6H13,n-hexyl C6H14,n-hexane C7H7,benzyl C7H8 C7H8O,cresol-mx
C7H14,1-heptene C7H15,n-heptyl C7H16,n-heptane C7H16,2-methylh C8H8,styrene
C8H10,ethylbenz C8H16,1-octene C8H17,n-octyl C8H18,n-octane C8H18,isooctane
C9H19,n-nonyl C10H8,naphthale C10H21,n-decyl C12H9,o-bipheny C12H10,biphenyl
HCN HCO HCCN HCCO HNC
HNCO HNO HNO2 HNO3 HCHO,formaldehy
HCOOH H2O2 (HCOOH)2 *N NCO
*NH NH2 NH3 NH2OH NO3
NCN N2H2 NH2NO2 N2H4 N2O
N2O3 N2O4 N2O5 N3 N3H
O3 C(gr) H2O(cr) H2O(L)

NOTE. WEIGHT FRACTION OF FUEL IN TOTAL FUELS AND OF OXIDANT IN TOTAL OXIDANTS

BIBLIOGRAPHY

[1] J.A. Vanderhoff and W. F. McBratney, “Burn-Rate Investigations of HAN-Based Candidate Liquid Propellants,” *US Army Rep.*, no. March, 1999.

[2] A. S. Gohardani *et al.*, “Green space propulsion: Opportunities and prospects,” *Progress in Aerospace Sciences*. 2014, doi: 10.1016/j.paerosci.2014.08.001.

[3] G. Derk, E. Boyer, G. Risha, R. A. Yetter, R. Dobbins, and M. . Smooke, “The Effect of Tube Diameter on the Burning Rate of Nitromethane as a Function of Pressure,” 2019.

[4] G. Derk, G. A. Risha, E. Boyer, and R. A. Yetter, “High-Pressure Burning Rate Measurements By Direct Observation,” *Int. J. Energ. Mater. Chem. Propuls.*, vol. 18, no. 3, pp. 213–227, 2019, doi: 10.1615/intjenergeticmaterialschemprop.2019028230.

[5] N. Klein, “Liquid Propellants for Use in Guns—A Review,” 1985.

[6] N. Wingborg *et al.*, “Development of ADN-based minimum smoke propellants,” in *46th AIAA/ASME/SAE/ASEE Joint Propulsion Conference and Exhibit*, 2010, doi: 10.2514/6.2010-6586.

[7] Y. P. Chang and K. K. Kuo, “Assessment of combustion characteristics and mechanism of hydroxylammonium nitrate-based liquid monopropellant,” *J. Propuls. Power*, vol. 18, no. 5, pp. 1076–1085, 2002, doi: 10.2514/2.6037.

[8] Q. Zhang and J. M. Shreeve, “Ionic liquid propellants: Future fuels for space propulsion,” *Chem. - A Eur. J.*, 2013, doi: 10.1002/chem.201303131.

[9] Q. Zhang and J. M. Shreeve, “Energetic ionic liquids as explosives and propellant fuels: A new journey of ionic liquid chemistry,” *Chemical Reviews*. 2014, doi: 10.1021/cr500364t.

[10] R. S. Jankovsky, “HAN-Based Monopropellant Assessment for Spacecraft,” 1996.

[11] B. D. Reed, “High-Performance Monopropellants and Catalysts Evaluated,” 2004.

[12] B. D. Reed, “HAN-Based Monopropellant Technology Development,” 2002.

[13] B. D. Reed, “On-Board Chemical Propulsion Technology,” *Tenth Int. Work. Combust. Propuls.*, no. April, 2004.

[14] C. Call, D. L. Zhu, C. K. Law, and S. C. Deevi, “Combustion and microexplosion of han-based liquid gun propellants at elevated pressures,” *J. Propuls. Power*, 1997, doi: 10.2514/2.5185.

[15] G. Sutton, Rocket Propulsion Elements, 6th ed., New York, NY: John Wiley and Sons, Inc., 1992.

[16] G. Derk, “High Pressure Burning Rates of JA2 and Nitromethane Propellants,” Master’s Thesis, University Park, PA: The Pennsylvania State University, 2019.

[17] T.L. Connell, “Combustion of HAN-based Propellants Containing Energetic Additives,” Unpublished Report, University Park, PA: The Pennsylvania State University, 2016.

[18] Y.P. Chang, “Combustion Behavior of HAN-Based Liquid Propellants,” PhD. Dissertation, University Park, PA: The Pennsylvania State University, 2002.

ACADEMIC VITA

Ezekiel Bugay

Mechanical Engineering honors student with skills in design, analysis, manufacturing and product implementation. Seeking to pursue a master's degree in propulsion following interests and notable academic research experience.

Relevant Experience:

Penn State University — State College, PA — 2019—Present

Undergraduate Research—High-Pressure Combustion Lab

- Research project with hydroxylammonium nitrate (HAN)-based propellants under Dr. Richard Yetter
- Investigation into behavior of propellant at extreme pressures using unique optical pressure chamber
- Observed combustion of HAN propellants in chamber with high speed camera; recorded burn rate as function of pressure
- Worked in a team of three to coordinate tests and repairs on equipment

Undergraduate Research—Additive Manufacturing

- Research project into behaviors of additively-manufactured lattice structures under Dr. Saurabh Basu
- Identified methods using photopolymer glues to strengthen and increase reliability of lattice structures
- Used FDM and SLA 3D printers to make samples; tested samples on a universal materials testing machine
- Presented findings at a university-wide convention on undergraduate research

Parker Hannifin (LORD Corp.) — Erie, PA — 2019

Mechanical Engineering Intern

- Estimated annual product margin increase with a new unique component design for drivetrain system
- Successfully proposed 10+ customer solutions, providing benefits such as reliability, safety, cost mitigation
- Created and administered three-part company-wide Additive Manufacturing training to engineers emphasizing faster functional prototyping, proper operation and safety, and printing self-sufficiency
- Worked with Additive Excellence team in exploring best practices and new uses of specialized thermoplastics.

Education:

Penn State University

BS in Mechanical Engineering, with Honors — 2021

- Senior, Schreyer's Honors College

Relevant Coursework:

Career and Technical Education — State College, PA — 2017—Present

Related Curriculum

Rocket propulsion, power cycles, fluid dynamics, heat transfer, machine design, differential equations, vibrations, finite element analysis, computer-aided design, computer programming

Other Work Experience:

Mid-West Rod and Restoration — Wapello, IA — 2014

Automotive Technician

- Assisted lead mechanic with classic car restorations—disassembly, body work, engine and transmission restoration, assembly and testing
- Employed special diagnostic tools to determine problems in the ignition, electrical and engine management systems
- Performed routine servicing on classic cars—fluid levels, brake and suspension inspections and repair, check major electrical and mechanical components in accordance with OEM and preventative servicing schedule.